IMPROVED LASER LOCKING TECHNIQUES FOR REALIZING AN ENHANCED MEASUREMENT OF THE HELIUM 2 TRIPLET P FINE STRUCTURE

HERMINA C. BEICA

A THESIS SUBMITTED TO THE FACULTY OF GRADUATE STUDIES
IN PARTIAL FULFILMENT OF THE REQUIREMENTS
FOR THE DEGREE OF

MASTER OF SCIENCE

GRADUATE PROGRAM IN PHYSICS AND ASTRONOMY
YORK UNIVERSITY
TORONTO, ONTARIO
OCTOBER 2013

IMPROVED LASER LOCKING TECHNIQUES FOR REALIZING AN ENHANCED MEASUREMENT OF THE HELIUM 2 TRIPLET P FINE STRUCTURE

by **Hermina C. Beica**

a thesis submitted to the Faculty of Graduate Studies of York University in partial fulfilment of the requirements for the degree of

MASTER OF SCIENCE

IMPROVED LASER LOCKING TECHNIQUES FOR REALIZING AN ENHANCED MEASUREMENT OF THE HELIUM 2 TRIPLET P FINE STRUCTURE

by **Hermina C. Beica**

Examination Committee Members:

1. Eric Hessels (Supervisor)
2. Cody Storry (Chair)
3. Scott Menary (Outside Member)

Abstract

The atomic fine-structure constant is a fundamental parameter that describes the coupling strength between charged particles and electromagnetic fields. Our group's objective is to measure this constant to an accuracy of 0.5 ppb based on precise measurements of the 2^3P_J fine-structure splittings of atomic helium. To measure the fine-structure splittings, we utilize an excitation scheme which requires two lasers locked to atomic resonances at wavelengths of 1083 nm and 707 nm. The accuracy of the fine-structure splitting measurement requires both laser frequencies to be stably locked to high precision. To achieve the desired accuracy of these laser locks, we have incorporated a saturated absorption setup in a dichroic atomic vapour laser locking (DAVLL) scheme. Using this locking technique, we have obtained a lock stability of ± 40 kHz for the 1083-nm laser and ± 140 kHz for the 707-nm laser, with the lasers remaining locked for a time scale of several weeks.

Acknowledgements

I would like to first thank my supervisor, Eric Hessels, for giving me the opportunity to work on such an interesting experiment. Throughout our discussions I was able to further my understanding of experimental physics and truly appreciate the art of precision measurements. His determination and efforts in explaining the related physics concepts helped me persevere through the difficulties and challenges faced during the experiment. I am truly grateful for all the help he provided.

I would also like to thank the three post-docs who helped me the most throughout the experiment: Amar Vutha, Matthew George, and Matthew Weel.

I would like to thank Amar for the long hours he put in to patiently explain the physics to me. His help and guidance throughout the experiment helped me learn so much, and most importantly, deepened my appreciation for the beautiful world of physics that surrounds us.

I would like to thank Matt George for introducing me to the experiment and for always taking the time to help me whenever I was faced with challenges. His

positive attitude and determination made the learning process that much more relaxing and enjoyable. And I also thank him for always taking the time to provide daily check-ups on my work.

I would also like to thank Matt Weel for taking the time to go over the details of the laser system, and for explaining the principles behind it. I truly appreciate the help and feedback he provided throughout the experiment.

I would like to thank Cody Storry, for his effective ideas and contributions during group meetings, and for allowing me to use (and borrow) his equipment whenever necessary.

I would also like to thank my lab mates for their help and support. I would like to thank Kosuke Kato for all the help and ideas he provided throughout the experiment. It was an absolute pleasure working with him. I would like to thank Imen Ferchichi for being such a great and true friend. I especially value all the great conversations we had along the way. I would like to thank Nikita Bezginov for always encouraging me to question the physics and search for the answers. And I would also like to thank Eric Davidson and Victor Isaac for making my time in the lab that much more enjoyable, and for the great conversations we had throughout. All of my lab mates have been incredible friends who have made my experience in the lab a memorable one.

I would like to thank Carol Guimaraes for being such a great and supportive

friend. I am very grateful for all the times she listened patiently to me in times of need, and also for the many laughs we shared throughout the years.

I would like to thank Adam Carew for lending me equipment when needed.

I would also like to thank Carson Mok for the feedback he provided regarding ECDLs. I really appreciate all his help.

I would like to thank Neema Afkhami-Jeddi for showing me how lasers are temperature cooled and pressure sealed.

I would also like to thank Frank Canzona for his help in using the machine shop, and Tyrone Lew for his help in building a subtraction detector.

I would like to thank Marlene Caplan for all her efforts regarding paperwork and keeping track of deadlines, for helping me sort out any administrative concerns, and for making my life a little easier. I would also like to thank Lauren O'Brien for her help whenever Marlene was unavailable.

And last, but certainly not least, I would like to thank my parents. Their understanding regarding my sometimes stressful and hectic schedule has made my journey immensely easier. And without their constant love and support I would not be where I am today.

Table of Contents

List of Tables

List of Figures

1 Motivation

This thesis presents improved laser locking techniques that will be applied towards a precision measurement of helium $n = 2$ triplet P fine-structure. A reduction in the frequency fluctuations of locked lasers is required to generate a stable detection signal for these measurements. Comparison between an improved high-precision measurement and high-precision theory will help determine the fine-structure constant (α) to high accuracy.

The fine-structure constant is a universal coupling parameter in the theory of quantum electro-dynamics (QED). The value of α is defined as

$$\alpha = \frac{e^2}{4\pi\epsilon_0\hbar c}, \tag{1.1}$$

where e is the elementary charge, ϵ_0 is the permittivity of free space, $\hbar$ is the reduced Planck constant, and c is the speed of light in vacuum. Since α characterizes the strength of electromagnetic interactions, it is important to know its value precisely for comparisons with QED theory [Aoyama et al. (2007), Hanneke et al. (2008)]. Recent theoretical calculations [Aoyama et al. (2012)] have succeeded in determin-

ing the electron g-2 factor to 0.25 parts-per-billion (ppb). The best experimental measurements of the g-factor [Hanneke et al. (2008)] are carried out by measuring the cyclotron frequency of an electron in a Penning trap. A comparison of g-2 calculations and experimental measurements is used to determine the value of α to a precision of 0.25 ppb [Aoyama et al. (2012)].

1.1 Helium fine structure interval measurements

Typically, atomic level structure calculations such as those for helium [Pachucki et al. (2012)] express atomic energy levels as a power series expansion of α. As a result, another approach for realizing a precise determination of α is from measurement of the fine-structure energy-level intervals in helium [Borbely et al. (2009), George et al. (2001), Smiciklas and Shiner (2010), Storry and Hessels (1998), Storry et al. (2000), Zelevinsky et al. (2005)]. Here, the best measurements [Smiciklas and Shiner (2010)] have realized a precision of 300 Hz for the fine-structure interval, which (with sufficiently precise theory) would correspond to a precision of 5 ppb for α. A measurement at York University [Borbely et al. (2009)], which has a precision of 350 Hz, uses the technique of separated oscillatory fields (SOF) [Ramsey (1949)]. Table 1.1 summarizes a history of precision measurements of the 2^3P energy intervals shown in figure 1.1.

The helium 2^3P fine-structure splittings are caused by contributions to the

Table 1.1: Measurements of the 2^3P fine-structure. Values are given in kHz, and numbers in parentheses are the uncertainties in the last digits.

Group/Year	$2^3P_2 \rightarrow 2^3P_1$	$2^3P_1 \rightarrow 2^3P_0$	$2^3P_2 \rightarrow 2^3P_0$
Hessels 1998 [Storry and Hessels (1998)]		29 616 966(13)	
Hessels 2000 [Storry et al. (2000)]	2 291 174.0(1.4)		
Hessels 2001 [George et al. (2001)]		29 616 950.9(0.9)	
Hessels 2009 [Borbely et al. (2009)]	2 291 177.53(35)		
Gabrielse 2005 [Zelevinsky et al. (2005)]	2 291 175.59(51)	29 616 951.66(70)	31 908 126.78(94)
Inguscio 2005 [Giusfredi et al. (2005)]	2 291 167.7(11.0)	29 616 952.7(1.0)	
Shiner 2010 [Smiciklas and Shiner (2010)]	2 291 175.9(1.0)	29 646 955.35(1.04)	31 908 131.25(30)

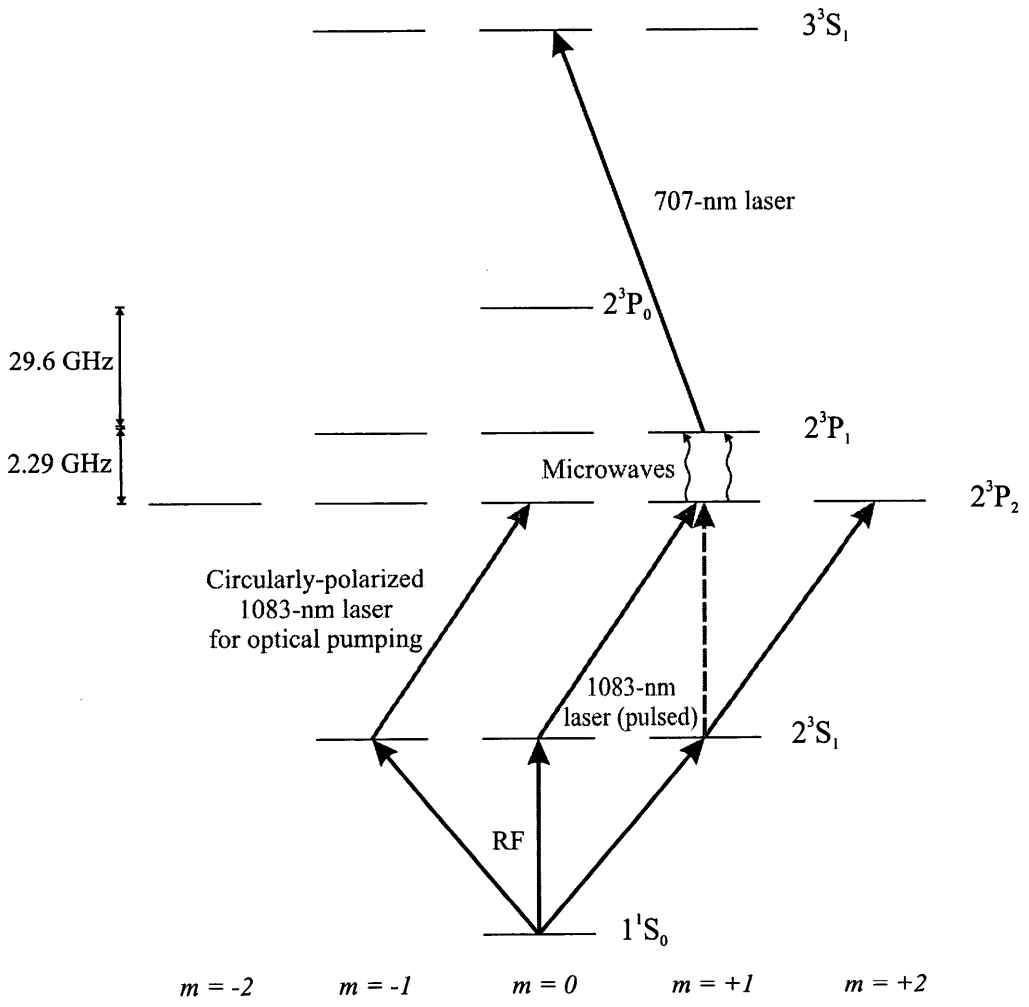

Figure 1.1: Helium excitation scheme. Energy level splittings are not to scale.

Hamiltonian that arise from the spin-orbit interaction and the spin-spin interaction in the two-electron system, as well as contributions from higher-order corrections due to relativistic and QED effects. There have been successive improvements in theoretical calculations which have determined higher-order correction terms to this splitting. Prominent theoretical work includes [Drake (2002), Pachucki and Sapirstein (2003), Pachucki and Yerokhin (2011)].

The helium energy-level diagram relevant to an ongoing precision measurement at York University is shown in figure 1.1. Helium atoms in an atomic beam are excited by an RF discharge from the 1^1S_0 ground state to the 2^3S_1 metastable state, which has a lifetime of 7800 s [Woodworth and Moos (1975)]. Atoms in the 2^3S_1 state are optically pumped using circularly polarized laser excitation at 1083 nm into the $2^3S_1(m = 1)$ magnetic sublevel. Pulsed laser excitation with linearly polarized 1083-nm light transfers the atoms to the $2^3P_2(m = 1)$ sublevel, which has a lifetime of 98 ns [Daley et al. (1972), Pichanick et al. (1968)]. Atoms in this level are subjected to two temporally separated pulsed microwave fields resonant with the $2^3P_2 \rightarrow 2^3P_1$ transition, allowing the energy interval to be measured using the SOF technique [Borbely (2009)].

The probability of excitation to the upper level as a function of the detuning from resonance for a single microwave pulse is a $sinc^2$ function (shown in blue in figure 1.2). The characteristic width of this pattern is $1/D$, where D is the

duration of the microwave pulse. The excited state probability as a function of detuning following excitation by two microwave pulses using the SOF method is shown in red in figure 1.2. The width of the central maximum is narrower and scales as $1/(2T)$, where T is the time separation between the two microwave pulses.

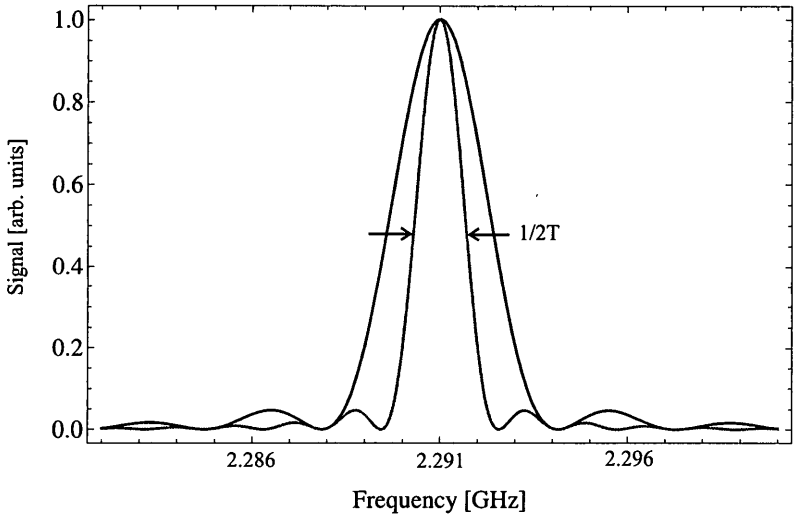

Figure 1.2: Microwave lineshapes. The 2^3P_1 population is shown as a function of detuning after excitation by a single pulse of microwaves (blue) and after two successive (SOF) pulses (red).

The $2^3P_1(m = 1)$ population after the two SOF pulses is determined by first laser exciting atoms in the $2^3P_1(m = 1)$ state to the $3^3S_1(m = 0)$ state using a 707-nm laser (figure 1.1). These atoms in turn decay to the 2^3P_J states through emission of 707-nm photons, and then to the 2^3S_1 state through the emission of 1083-nm photons. The resulting atoms in the $2^3S_1(m = -1)$ sublevel are measured

using deflection by a Stern-Gerlach magnet. Only atoms that undergo the SOF transition can end up in this $m = -1$ metastable state.

A 1083-nm laser can also be used to laser cool an atomic helium beam. The diverging helium beam can be collimated by 1083-nm light sent along transverse directions with respect to the direction of the beam [Rooijakkers et al. (1996)]. Such cooling allows for a more parallel and more intense beam of metastable helium atoms.

The goal of this thesis is to support the ongoing precision measurement of the helium fine-structure splittings in our group, which has a targeted precision of 30 Hz. The thesis focuses on methods to lock the laser frequencies of the 1083-nm and 707-nm lasers used to excite the helium atoms. The work described here will enable helium experiments to operate with a higher signal-to-noise (S:N) ratio. The laser frequency stability associated with the 1083-nm transition will result in more stable laser cooling, which will allow the intensity of the laser-cooled beam to be more stable. Additionally, the stability of optical pumping and of laser excitation into the 2^3P_2 energy level will be enhanced and the stability of laser excitation of the $2^3P_1 \rightarrow 3^3S_1$ transition at 707 nm will be improved, leading to better detection stability. The improved stability will lead to less fluctuation in the signals and therefore better S:N.

In chapter 2 of this thesis, the fundamental requirements for frequency locking

of the 1083-nm and 707-nm lasers using resonance lines in a helium reference cell are introduced. In the following chapters, three types of laser frequency stabilization methods are developed and characterized: the saturated absorption technique covered in chapter 3, the DAVLL (dichroic atomic vapour laser lock) technique covered in chapter 4, and the DS-DAVLL (Doppler-selective-DAVLL) technique covered in chapters 5 and 6. Each chapter presents the details of the experimental setup and discusses the results of the laser locking. Lastly, chapter 7 addresses the potential for additional improvements.

2 Introduction

In this chapter, the two laser systems used in the experiment are described, and the characteristics of a dispersion-shaped error signal are introduced. The chapter concludes with a description of the LabVIEW interface and the locking parameters used in stabilizing the laser frequencies.

2.1 Description of laser systems

Diode lasers are used extensively in this work. A laser diode consists of a pn-junction fashioned in the form of an optical cavity. An injection current leads to radiative recombination of holes and electrons. The radiation is amplified by the internal cavity of the laser diode. It is possible to coarse-tune the laser frequency by changing the temperature of the laser diode or by changing the injection current. Both the temperature and the current affect the internal laser cavity [Träger (2007)].

2.1.1 The 1083-nm laser

The laser diode used for driving the 1083-nm transition in helium has a distributed-Bragg reflector (DBR) cavity. The laser diode used for the saturated absorption and DAVLL techniques is an SDL-6702-H1 diode, while the DS-DAVLL technique uses a Photodigm PH1083DBR080T8 diode. The DBR laser diode is current- and temperature-controlled by a Melles-Griot 06 DLD 203/IEEE controller. For a DBR diode laser, a grating is integrated into the material of the diode [Träger (2007)]. The grating makes the frequency of the light output by the laser less susceptible to mechanical vibrations. The Photodigm laser diode has a linewidth of approximately 1.5 MHz, and the SDL linewidth is approximately 3 MHz. The maximum power output generated with the Photodigm laser diode is 50 mW at an applied current of 126 mA and the SDL diode has a maximum output of 15 mW at 124 mA. The temperature of the Photodigm diode is set at 27°C, and has a specified tuning rate of 19 MHz/mK (and the SDL diode would be expected to have a similar tuning rate). More 1083-nm laser power is available by using a NuFERN 1064-to-1110-nm single-frequency (Gen. II) fiber amplifier, capable of outputting 15 W of power with an input laser power of $\sim$10 mW.

The laser frequency can be modulated by applying a time-varying voltage to the current-adjust input of the laser controller. The current-adjust input causes

a current tuning of 62 mA/V. Typically, a voltage divider is placed in front of the current-adjust input to give a smaller amplitude of frequency modulation. The laser frequency can be scanned across the $2^3S_1 \rightarrow 2^3P_1$ and $2^3S_1 \rightarrow 2^3P_2$ resonances (refer to figure 3.6). Based on the known 2.29-GHz frequency difference between the 2^3P_1 and 2^3P_2 states, and the fact that a factor-of-168 voltage divider is used, a conversion factor of 37 MHz/mV is determined for the Photodigm laser. The SDL laser tuning rate is determined to be very similar: 35 MHz/mV. That is, the laser is tuned by 37 MHz (or 35 MHz for the SDL diode) for each millivolt of additional voltage applied to the current-adjust input.

The 1083-nm laser controller also allows for frequency tuning by applying a voltage to a temperature-adjust input. This input changes the diode temperature at a rate of $\sim$0.5 mK/mV and the temperature tuning rate for this input is measured to be 10 MHz/mV (19 MHz/mV for the SDL diode). This means that 1 mV of additional voltage applied to the temperature-adjust input of the laser controller corresponds to a 10 MHz (or 19 MHz for the SDL diode) change in laser frequency. Our locking schemes send corrections to the temperature-adjust input, which has a response time of about 2 seconds, which implies a bandwidth of 0.5 Hz. The current-adjust input has a faster response time ($\sim$1 μs); however, we find it unnecessary to lock with a faster response time.

2.1.2 The 707-nm laser

The 707-nm laser is an external cavity diode laser (ECDL) (model DL 100 from Toptica), which has a length of 3 cm, so that the mode spacing ($c/2L$) is 5 GHz. The internal diode cavity is only 2 mm in length, corresponding to longitudinal modes spaced at 80 GHz. Optical feedback from this internal cavity leads to the exponential growth of preferred cavity modes, which creates a narrow linewidth emission. A grating (with line spacings of 1.6 μm) is placed in the external cavity to select and feed back a narrow range of frequencies.

The 707-nm ECDL is based on a Littrow design, outlined in figure 2.1. The zeroth-order reflection from the grating constitutes the laser output, and the first-order diffracted beam is fed back to the laser diode to narrow the laser linewidth. In addition to temperature and current tuning, it is also possible to adjust the frequency of this laser by varying the length of the external cavity and the grating angle. This is accomplished by changing the voltage supplied to a piezoelectric transducer (PZT) attached to the grating. For mode-hop-free tuning and scanning of the laser, it is necessary to shift the internal cavity modes synchronously with the external cavity modes using a feed-forward circuit. If the internal and external cavity modes are not shifted at the same time, the laser will no longer operate in a single mode.

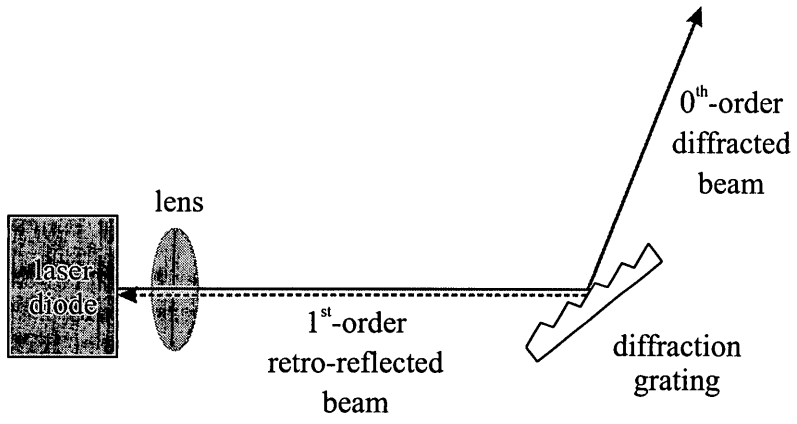

Figure 2.1: Block diagram of a Littrow-configuration diode laser.

The 707-nm laser is powered by a DL 100 Toptica controller. The diode used in our laser head is an InGaAsP laser diode (HL7001MG) purchased from Thorlabs. The diode operates between 700 and 710 nm, with a maximum output power of 40 mW at the central wavelength of 705 nm. For our desired 707-nm wavelength, we are able to obtain a power output of 30 mW at a typical operating current of 75 mA and case temperature of 30.2°C.

Because the 707-nm laser is an ECDL, feedback from the grating into the diode must be optimized for single-mode operation. To test the operating range of the laser, the PZT is first scanned by supplying a time-varying voltage to the PZT control voltage input. The scan is applied across a large frequency range, typically 2-4 GHz. It is necessary to tune the current, temperature, and feed-forward parameter to ensure a mode-hop-free scan range. The feed-forward parameter determines the ratio of the control voltage for the PZT to the voltage applied to the current-

adjust input. For our operating conditions, the feed-forward is set by a front-panel adjustment at a factor of 1/4. The response time for this frequency tuning is less than 1 ms, which results in a bandwidth greater than 1 kHz. For the 707-nm laser locking techniques described in this thesis, the correction voltage required to stabilize the laser frequency is applied to the PZT control voltage, and the internal current-adjust is controlled by the feed-forward control.

Frequency monitoring with a Burleigh WA-1500 wavemeter is helpful in maintaining the coarse tuning of the laser frequency. We also rely on this wavemeter to calibrate the rate of frequency tuning versus applied voltage to the PZT control (see figure 2.2). The result of this measurement is a 1.3 MHz/mV tuning factor, which implies that the laser frequency changes by 1.3 MHz for each millivolt of additional voltage applied to the PZT control voltage input.

2.2 Helium cells used for frequency locking

Our locking techniques are based on an excitation scheme outlined in figure 2.3. First, ground-state 1^1S_0 helium atoms inside a glass cell are driven to the 2^3S_1 metastable state with an RF discharge. The helium pressure in the cell is between 300 and 500 mTorr. Two copper rings are wrapped around the ends of the helium cell to drive the RF discharge. A 1083-nm laser beam excites 2^3S_1 metastable helium atoms in the cell to the 2^3P_2 state, where they can further interact with the

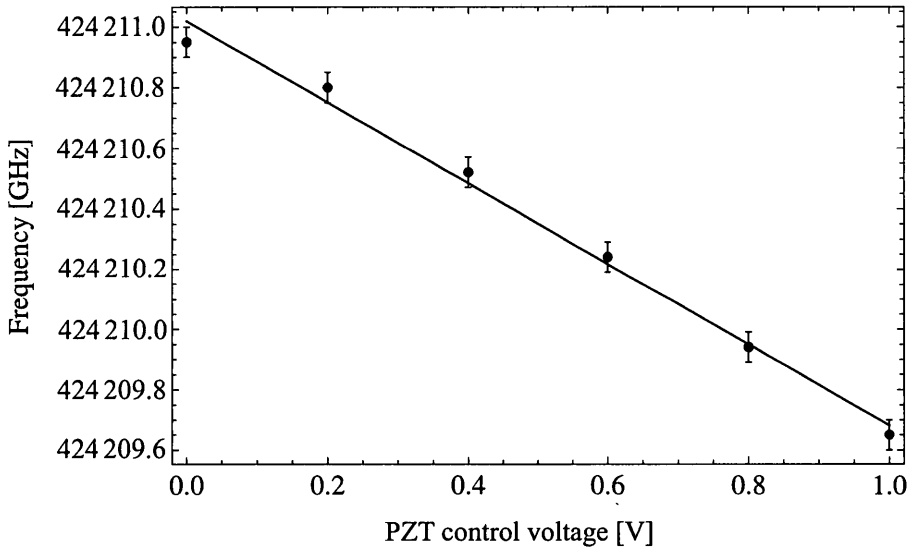

Figure 2.2: 707-nm voltage-to-frequency calibration. Calibration plot showing frequency measured by the wavemeter as a function of PZT control voltage.

707-nm laser, which drives atoms to the 3^3S_1 state.

Experiments described in this thesis use glass cells which have a diameter of 2 cm and a length of 10 cm. We found that for a frequency lock of the 1083-nm laser, optimal pressures are between 300-400 mTorr, while for the 707-nm laser optimal pressures range from 400-500 mTorr.

The spectrum of the helium discharge is examined using an Ocean Optics USB2000+ Miniature Fiber Optic spectrometer with a resolution of 1 nm. Figure 2.4(a) shows the spectrum of the cell used for locking the 1083-nm laser with the saturated absorption, DAVLL, and DS-DAVLL techniques. This particular cell is also used to lock the 707-nm laser in the saturated absorption technique. Figure

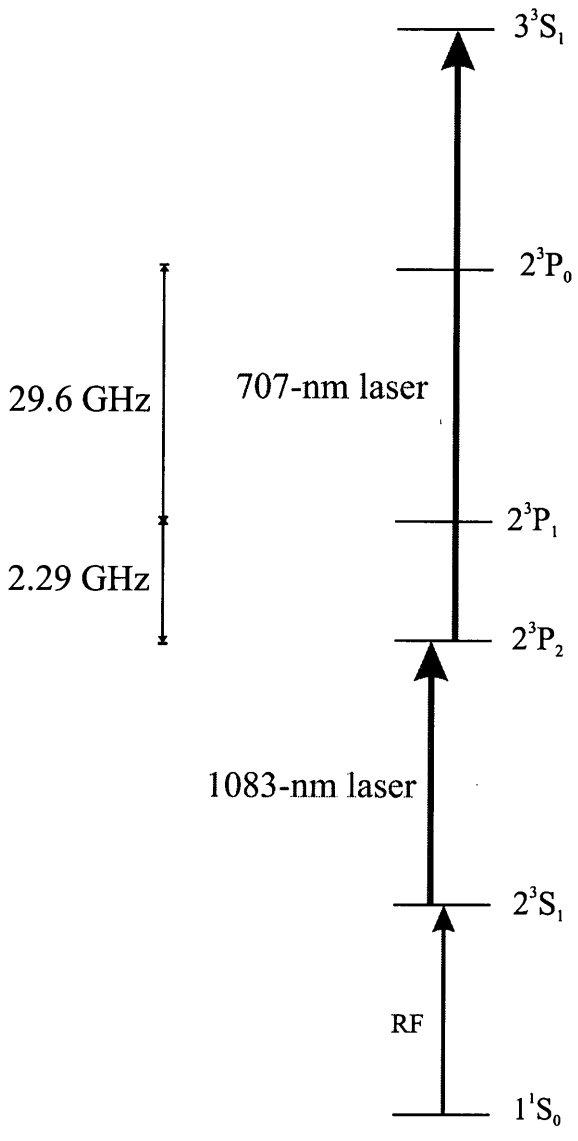

Figure 2.3: Excitation scheme used for laser locking. (Energy levels are not to scale).

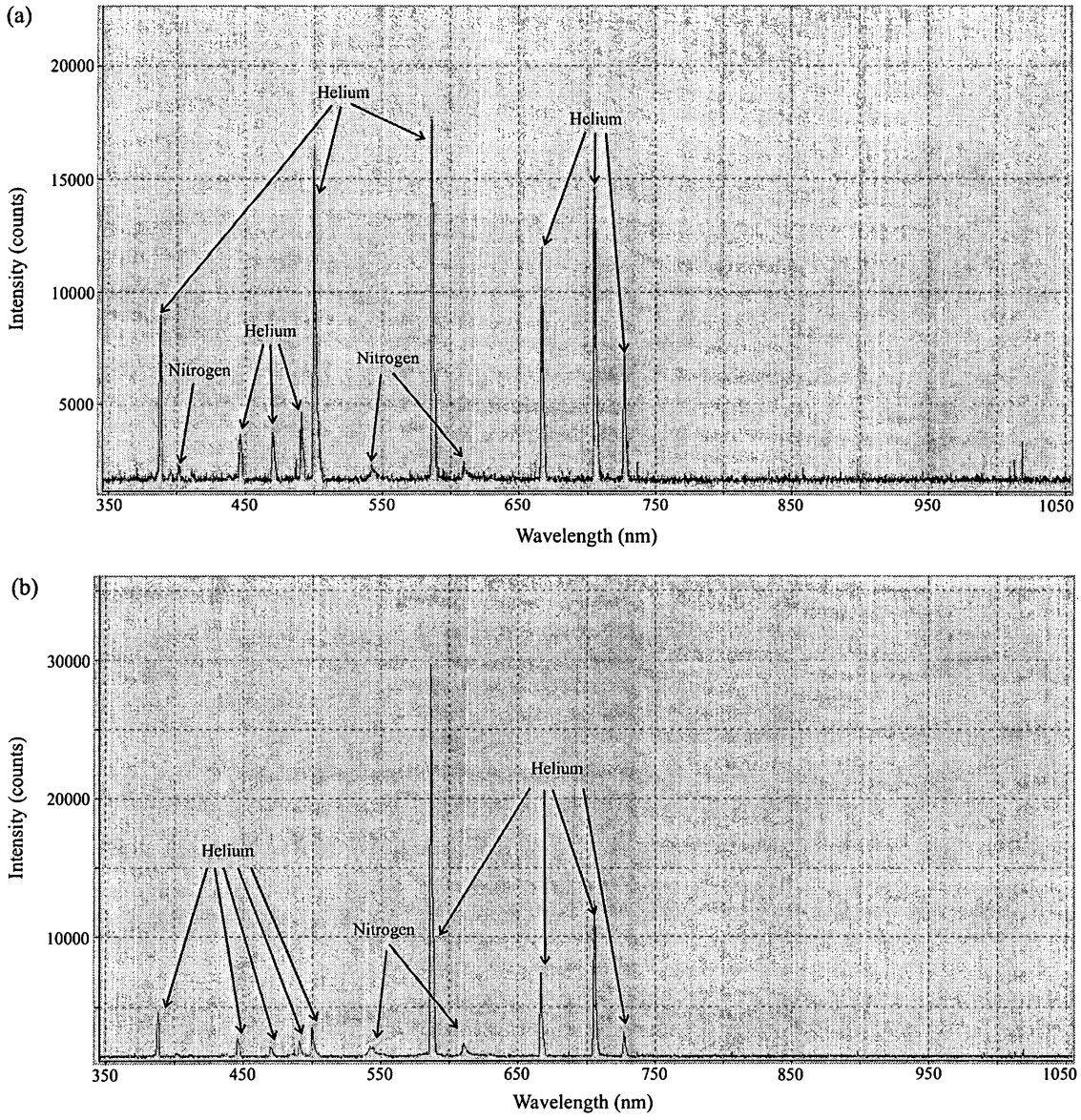

Figure 2.4: Spectra of the helium vapour cells. (a) Spectrum of helium discharge for the 1083-nm reference cell. (b) Spectrum of helium discharge for the 707-nm reference cell.

2.4(b) shows the spectrum of the helium cell used for locking the 707-nm laser with the DS-DAVLL technique. The spectra have a wavelength range of 350 nm to 1050 nm, determined by the limits of the spectrograph. All the prominent spectral lines corresponded to well-known transitions in helium, suggesting that the helium cells contain a high purity of helium gas.

2.3 Requirement and characteristics of an error signal

A free-running diode laser exhibits frequency drifts due to, for example, ambient temperature fluctuations, ambient pressure variations, and laser current noise. The goal of this thesis is to lock the laser frequency by observing and compensating for these fluctuations, thus reducing the laser frequency drifts. The challenge for laser frequency stabilization is to devise a detection technique which produces a dispersion-shaped error signal (such as the one shown in figure 2.5) that can be used to stabilize the laser frequency to an atomic resonance. This dispersion signal is typically generated by tuning the laser frequency across an atomic transition in a reference vapour cell. The dispersion signal can be used to determine the frequency correction required to keep the laser at the resonant frequency, which occurs at the zero-crossing of this dispersion. Such a dispersion feature is at the heart of any feedback loop used for laser locking. Figure 2.6 shows the block diagram for a characteristic feedback loop.

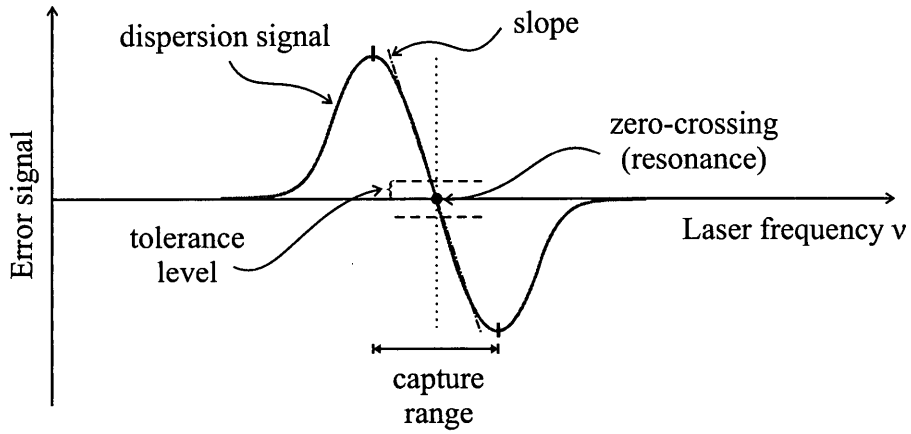

Figure 2.5: Characteristics of a dispersion-shaped error signal.

There are two main characteristics of the dispersion signal that affect the quality of a laser lock: the slope and the capture range, as shown in figure 2.5. The first of these characteristics – the slope of the dispersion signal – provides the frequency-to-voltage conversion factor used for correcting the laser frequency. A steeper slope results in larger signals for determining how far the laser is from resonance.

The second characteristic – the capture range – determines the frequency range over which the feedback loop can effectively output a correction to the laser. If the laser frequency drifts outside of this capture range, the feedback loop is not effective at bringing the frequency back onto resonance, and the lock is thus said to be broken. As a result, a large capture range is desirable, as it ensures that the laser remains locked for extended periods of time, even when the laser frequency drifts or noise is present in the error signal. However, a large capture range can

also lead to a decrease in the steepness of the slope. Thus, a trade-off between the two must be made when optimizing the dispersion signal.

To determine the quality of a laser frequency lock the quantity σ_{lock} is calculated. This quantity is determined from the standard deviation of a series of one-second averages of the error signal (of figure 2.5) divided by the slope of the dispersion signal, shown in figure 2.5. Thus σ_{lock} (which has units of MHz) is a measure of how far the laser frequency fluctuates from resonance (after averaging over one-second time periods) when the laser lock is engaged.

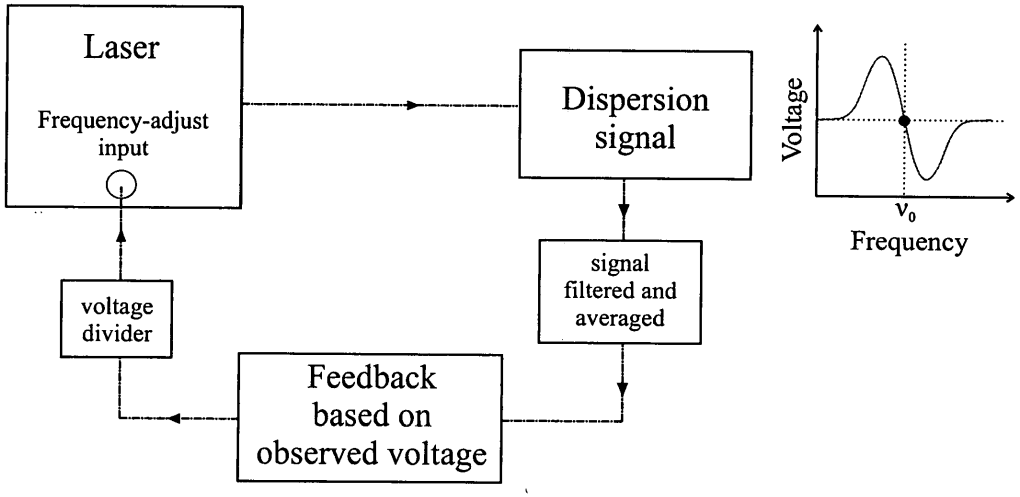

Figure 2.6: Block diagram of a laser locking feedback loop.

2.4 The LabVIEW program

Chapters 3, 4, 5, and 6 describe laser locking with saturated absorption, DAVLL and DS-DAVLL techniques. The feedback mechanism required to correct the laser frequency is operated by a LabVIEW software program. This interface uses a number of input parameters to calculate the correction voltage required to stabilize the laser frequency.

The LabVIEW program reads an error voltage (the error voltage of figure 2.5) through the use of an analog-to-digital converter (ADC). The program acquires and averages 50 readings every second before applying a correction (at a rate of one correction per second) to the laser frequency via a digital-to-analog converter (DAC). The ADC input and DAC output channels are part of a measurement and automation device called a LabJack, which communicates with the LabVIEW program through a USB computer connection. A LabJack U3 (with 12-bit inputs and 10-bit outputs) is used for the saturated absorption technique and a LabJack U6-Pro (with 18-bit inputs and 12-bit outputs) is used for the DAVLL and DS-DAVLL techniques. A low-pass (LP) filter is used before the error signal goes to the ADC input, so that any high-frequency noise in the error signal does not contribute to the LabJack readings.

When engaging the LabVIEW program for the laser lock, the user must select

two main locking parameters: the tolerance level and proportional gain. The first parameter – the tolerance level – determines how far the laser frequency is allowed to drift away from resonance (see figure 2.5) before the program applies a correction. Ideally, this value would be zero, but noise in the error signal makes a finite value reasonable. The tolerance level must be small to obtain a good lock on the laser frequency.

The second parameter – the proportional gain – represents the magnitude of the correction voltage required to tune the laser frequency back onto resonance. If the error voltage is greater than the tolerance, the program multiplies the proportional gain parameter with the measured error voltage to calculate a correction voltage. This correction voltage is generated by the DAC of the LabJack and, after passing through a voltage divider, is sent to the frequency-adjust input of the laser being stabilized, as shown in figure 2.6. The applied correction brings the frequency closer to resonance which, in turn, lowers the value of the error voltage. When the feedback loop is engaged, the LabVIEW program plots the error voltage values streamed by the LabJack. Each point in the plot corresponds to the average of 50 LabJack readings (averaged over a period of one second). It is on the basis of these one-second averages that the LabVIEW program computes the necessary correction voltage for the laser frequency.

The LabVIEW program calculates the standard deviation of the error voltage

for a large number of one-second averages. Dividing this standard deviation by the slope of the dispersion curve in figure 2.5 gives the σ_{lock} value for the frequency lock.

A larger-amplitude dispersion feature leads to a better S:N ratio for the lock, which can result in a smaller σ_{lock}. It is important to note that the noise in the error signal (and therefore σ_{lock}) is a combination of frequency noise (determined by the frequency stability of the laser) and electrical noise picked-up by the electronics used in the locking feedback loop. Averaging over one second helps to eliminate much of this electrical noise, and the aim is to have σ_{lock} be mainly determined by the frequency stability of the laser.

3 Saturated absorption spectroscopy

3.1 Introduction to saturated absorption

A popular method used for laser frequency stabilization is the technique of saturated absorption spectroscopy. For a vapour cell, laser absorption spectra are Doppler broadened due to the Maxwell-Boltzmann velocity distribution. Its one-dimensional form along the axis of the laser beam is given by [Träger (2007)]:

$$f(v_z) = n\sqrt{\frac{m}{2\pi k_B T}}e^{-\frac{mv_z^2}{2k_B T}}, \tag{3.1}$$

where n is the number density, m is the atomic mass, k_B is the Boltzmann constant, and T is the equilibrium temperature.

The first-order Doppler frequency shift is given by [Demtröder (2008)]

$$\nu_D - \nu_L = \nu_L \frac{v_z}{c}. \tag{3.2}$$

In the above equation, ν_D is the Doppler-shifted frequency, ν_L is the laser frequency, and c is the speed of light in vacuum. Atoms moving towards or away from the laser

propagation direction see the laser light Doppler shifted above or below resonance, respectively.

Second-order Doppler-shifts can be ignored because the velocity of the helium atoms near room temperature (approximately 1300 m/s) is much smaller than the speed of light.

Laser excitation of the gas in the vapour cell produces a Gaussian spectral profile. Using equations 3.1 and 3.2, it is possible to show that this profile has a width of

$$\Delta\nu_{FWHM} = \frac{\nu_0}{c}\sqrt{\frac{2k_BT\ln 2}{m}}, \tag{3.3}$$

where $\Delta\nu_{FWHM}$ is the characteristic full-width at half-maximum (FWHM) of the line profile [Demtröder (2008)], and ν_0 is the resonant frequency for the transition.

The Gaussian shape (see figure 3.1) corresponding to the 1083-nm transition

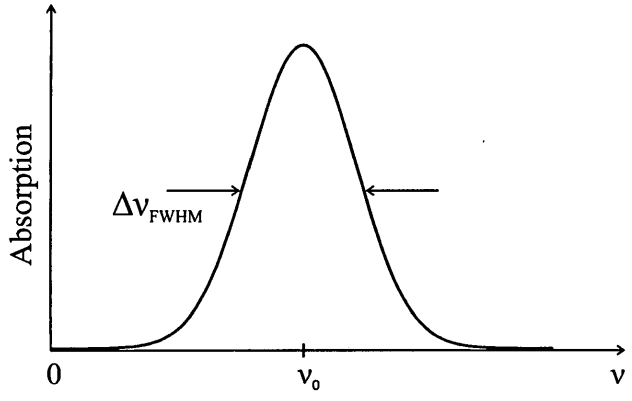

Figure 3.1: Absorption spectrum of a two-level atom due to the velocity distribution.

between the 2^3S and 2^3P states has a FWHM of approximately 1.3 GHz for our room-temperature helium atoms. The saturated absorption technique allows lasers to address only the class of atoms for which v_z is approximately zero, and produces a narrow lineshape that can be used as a more precise reference for laser locking.

For the saturated absorption technique, two counter-propagating laser beams derived from the same laser (a strong pump and a weak probe) are anti-aligned through the reference cell along the **z**-axis (figure 3.2). If the laser frequency does not coincide with the resonant frequency, the two beams will excite atoms in two different velocity groups (centered at $\pm v_z$). Atoms with these velocities will be Doppler-shifted onto resonance. As a result, two classes of atoms will be depleted by the laser, as shown by the velocity distribution in figure 3.3.

If the laser frequency coincides with the resonant frequency of the atoms (ν_0), both pump and probe beams address the same group of atoms (those with $v_z \sim 0$). The intense pump beam with $I \sim 10I_{sat}$ (where $I_{sat} \sim 0.2$ mW/cm^2 is the charac-

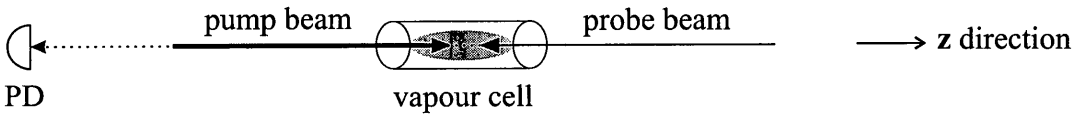

Figure 3.2: Basic configuration for saturated absorption. After passing through the vapour cell, the probe beam power is detected by a photodiode (PD) to generate an absorption signal.

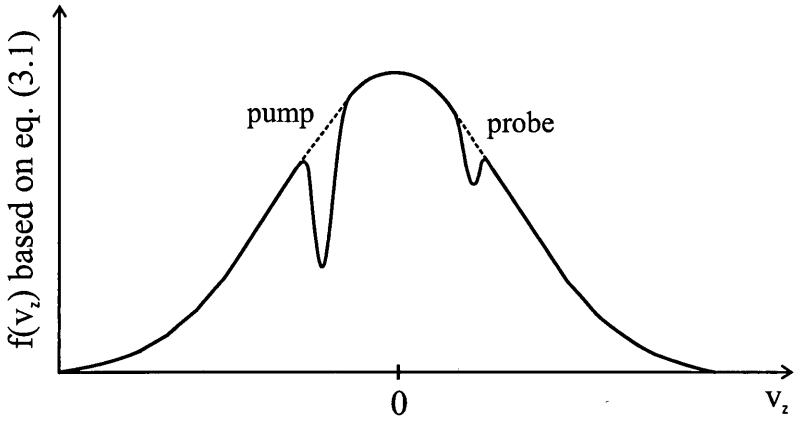

Figure 3.3: Holes in the velocity distribution curve of the 2^3S_1 state. The holes correspond to the case for which $\nu_L < \nu_0$, where ν_L is the laser frequency in the lab frame. The pump and probe alignment is shown in figure 3.2. The velocity is related to the frequency as per equation 3.2.

teristic saturation intensity for the 1083-nm transition), leads to a high absorption rate of the atoms from the 2^3S_1 state. Since the 2^3S_1 state becomes sufficiently depleted (saturated), the absorption of the probe beam is reduced, hence the name saturated spectroscopy. The reduction in the probe absorption in the presence of the pump beam leads to a narrow spectral feature known as the Lamb dip [Demtröder (2008)] (see figure 3.4), which can be used for laser frequency locking.

Because the Lamb dip represents a Doppler-free absorption profile, its width could be as narrow as the natural linewidth of the transition (in this case 1.6 MHz). In practice, however, the profile is broadened by a number of effects, including power broadening and collisional broadening [Demtröder (2008)].

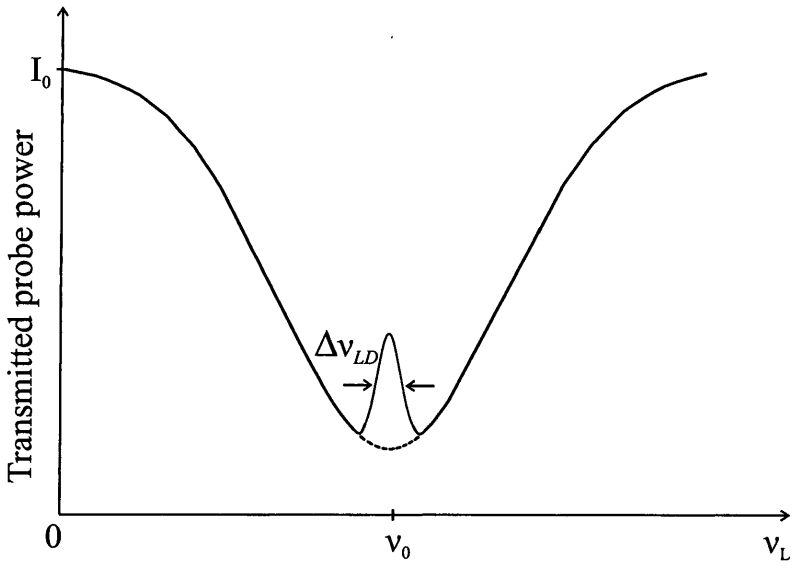

Figure 3.4: The Lamb dip in a Doppler-broadened spectrum. The probe absorption spectrum shows the zero-velocity class addressed by both pump and probe beams for the case $\nu_L = \nu_0$. Here, $\Delta\nu_{LD}$ ~40 MHz, where $\Delta\nu_{LD}$ is the FWHM of the Lamb dip.

3.2 Experimental setup of the 1083-nm laser

The experimental setup for saturated absorption using the 1083-nm laser is outlined in figure 3.5. The powers of the pump and probe beams are 60 μW and 20 μW, corresponding to intensities of $\sim$3 mW/cm^2 and $\sim$1 mW/cm^2, respectively. After passing through the cell, the probe beam is focused to a spot size much smaller than the 31-mm^2 active area of a Melles-Griot silicon photodiode (13 DSI 009). This photodiode, along with a Melles-Griot (Large Dynamic Range) current amplifier measures the power of the probe beam after if passes through the cell.

The laser frequency can be scanned across the $2^3S_1 \rightarrow 2^3P_2$ atomic transition by

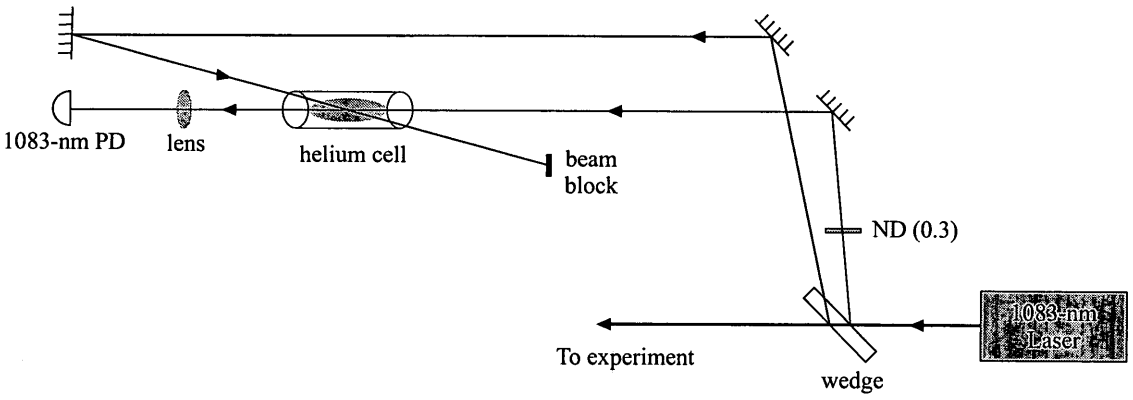

Figure 3.5: Experimental setup for saturated absorption with the 1083-nm laser. Here, PD refers to a photodiode, and ND represents a neutral density filter. The angle between the two laser beams passing through the helium cell is exaggerated for clarity. In the actual setup, the laser beams are within 10 mrad of anti-parallel with respect to each other.

a 400 Hz triangle wave provided by an Agilent 33120A function generator to show the Lamb dip signal. The triangle wave is sent through a factor-of-168 voltage divider to the current-adjust input of the laser controller. Figure 3.6 shows an oscilloscope trace (blue) of the Doppler-free resonances corresponding to the $2^3S_1 \rightarrow 2^3P_2$ and $2^3S_1 \rightarrow 2^3P_1$ transitions. The yellow trace represents a scan ramp of 4 GHz applied to the current control. By using the calibration factor of 35 MHz/mV (see section 2.1.1), the width of the Doppler-broadened profile is inferred to be approximately 1.5 GHz and the width of the Lamb dip for the stronger $2^3S_1 \rightarrow 2^3P_2$ transition is inferred to be approximately 40 MHz.

A Lorentzian fit corresponding to the Lamb dip of the $2^3S_1 \rightarrow 2^3P_2$ transition

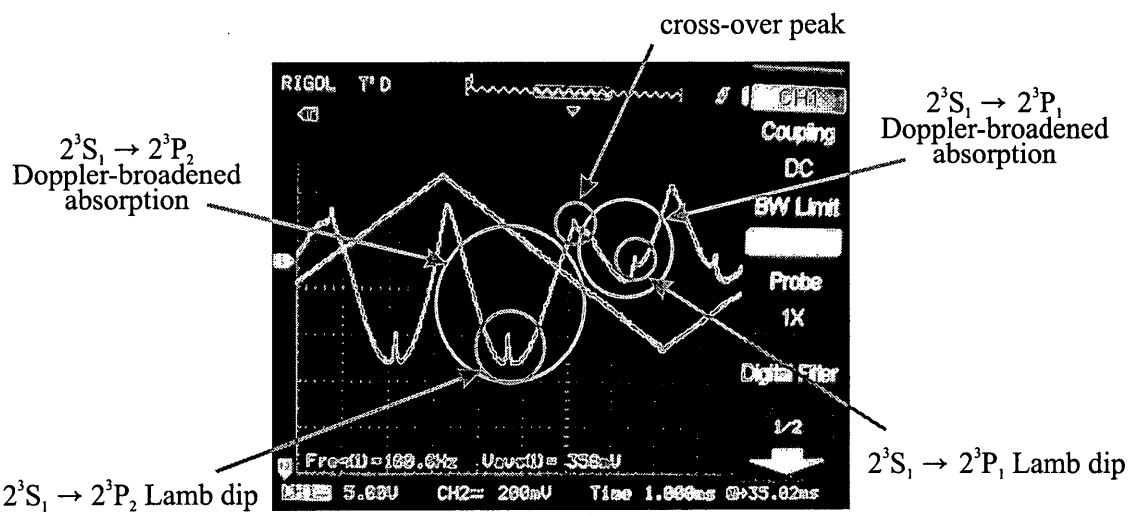

Figure 3.6: Oscilloscope traces for obtaining 1083-nm Lamb dips. Shown are the scan ramp applied to the laser current and the Lamb dips for the 1083-nm transitions.

is shown in figure 3.7(a). The first derivative of this Lorentzian lineshape, shown in figure 3.7(b), has the form of a dispersion curve which can be used for locking the laser frequency. This derivative can be obtained by applying a small-amplitude frequency modulation along with a lock-in amplifier.

To obtain the small-amplitude frequency oscillation, the peak-to-peak scan amplitude is reduced (with the aid of a factor-of-750 voltage divider) to 0.3 mV (corresponding to a peak-to-peak frequency modulation of 10 MHz). The current-amplified photodiode signal is sent to the input of a lock-in amplifier (EG&G Princeton Applied Research, Model 128A), as outlined in figure 3.8. The TTL output of the function generator serves as the reference input signal for the lock-in amplifier (figure 3.8). The lock-in amplifier output passes through an internal low-pass filter of 3 Hz. This filtered lock-in output forms the error signal for the lock. The resulting dispersion curve of this error signal is similar to the curve of figure 3.7(b), and has a capture range and a slope (as defined by figure 2.5) of $\sim$30 MHz and 2.8 mV/MHz, respectively. The error signal is read by the LabVIEW program with the aid of the ADC input of a LabJack U3. The inputs of this LabJack have a 12-bit resolution on a 5-V range, meaning that the least-significant bit (LSB) of the ADC has a voltage step of 1.2 mV (corresponding to a frequency of $\sim$400 kHz). The LabVIEW program averages 50 LabJack readings every second. The LabVIEW program computes a correction voltage based on the proportional gain

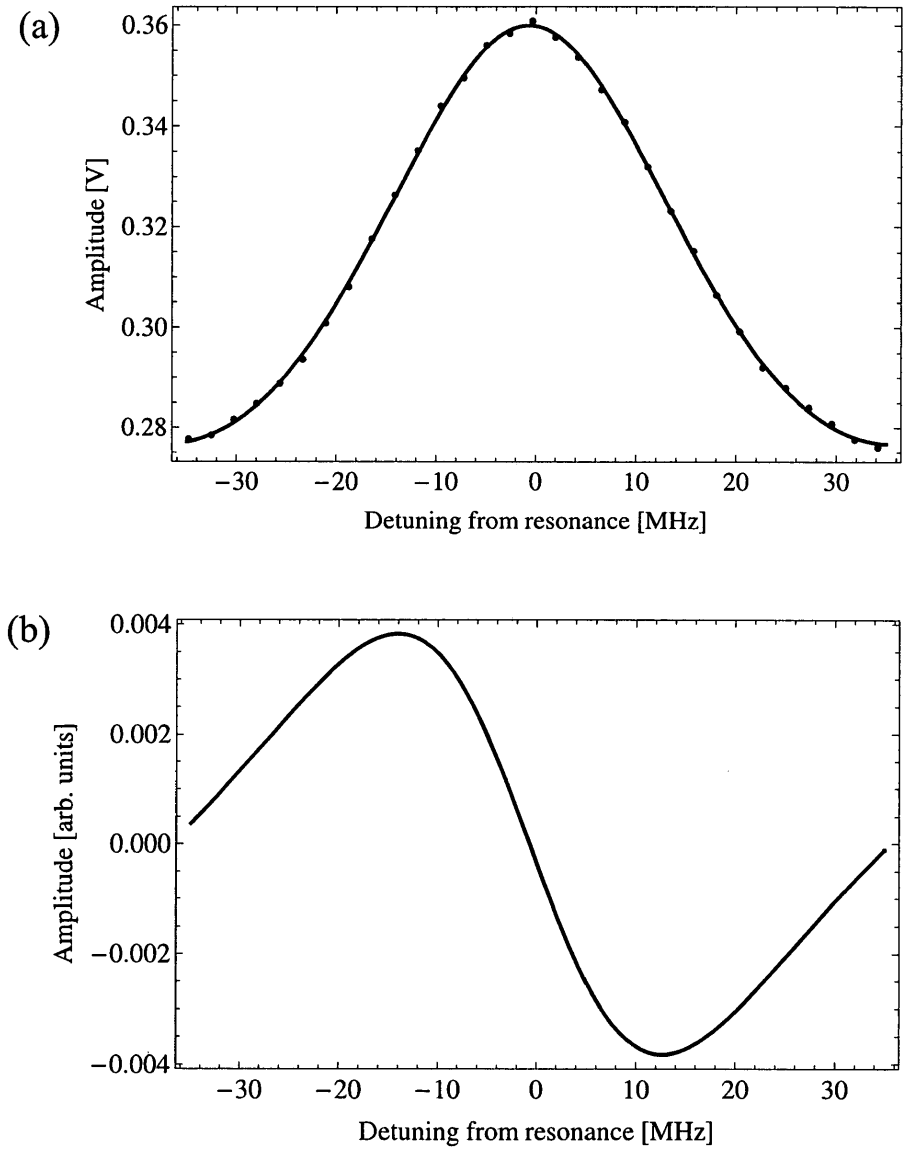

Figure 3.7: Locking signals for the 1083-nm saturated absorption technique. (a) Lorentzian fit to the Lamb dip for the $2^3S_1 \rightarrow 2^3P_2$ transition. (b) Dispersion curve corresponding to the first derivative of the $2^3S_1 \rightarrow 2^3P_2$ Lamb dip.

and tolerance setting. The proportional gain for this locking scheme is typically set to a value of 0.3. This proportional gain parameter is approximately the reciprocal of the product of the slope of the dispersion curve (2.8 mV/MHz) and the laser frequency temperature tuning factor after the factor-of-22 voltage divider of figure 3.8 (19/22 MHz/mV).

The tolerance level of the LabVIEW program is typically set at a value of 10 mV, corresponding to approximately 4 MHz. This tolerance setting gives the best stability of the locked error signal, and lower settings show no improvements in

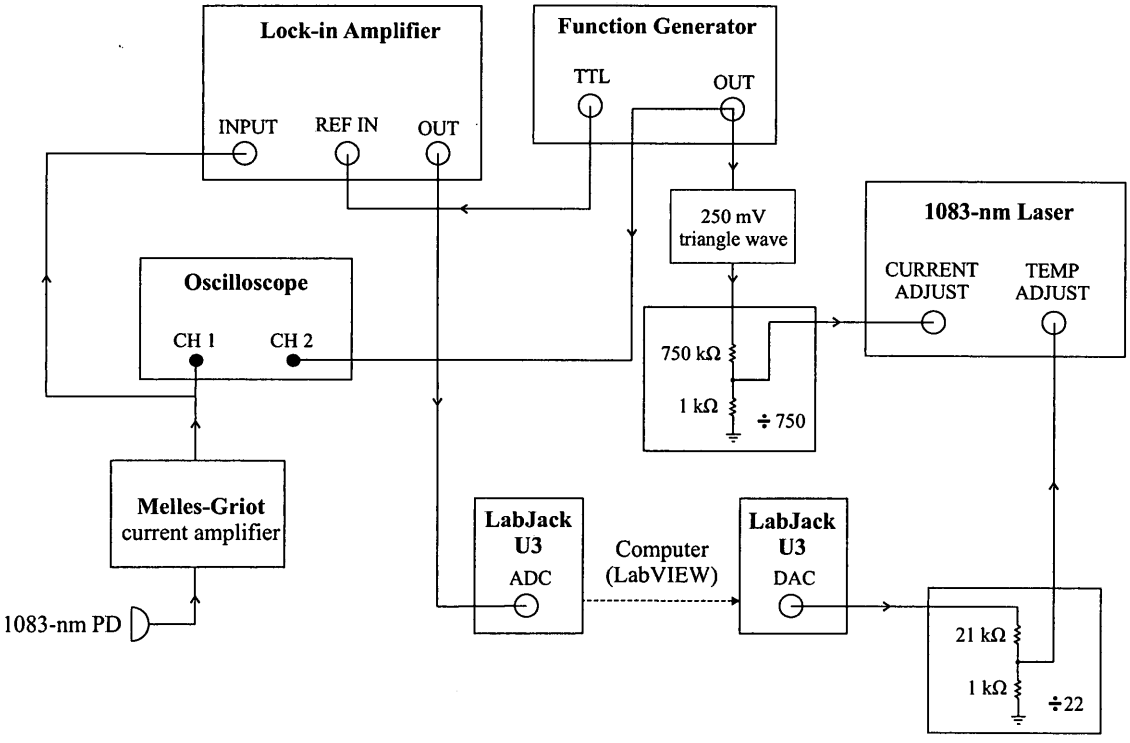

Figure 3.8: Feedback loop of the 1083-nm laser system.

the laser lock. Every second, the output correction voltage computed in software is sent from the DAC of the LabJack, which has a resolution of 10 bits on a 5-V range. To compensate for the limited DAC resolution, the correction voltage passes through the factor-of-22 voltage divider, resulting in a LSB voltage of 0.2 mV, corresponding to a frequency of 4 MHz. This divided correction voltage is applied to the temperature-adjust input of the laser controller. The full 5-V tuning range of the DAC corresponds to a frequency range of 4.3 GHz.

3.3 Results of the 1083-nm laser

Based on the standard deviation of the 1-s averages of the error signal computed in LabVIEW (when the 1083-nm laser is locked for periods of a few hours) and the 2.8 mV/MHz slope of the dispersion curve, the value determined for σ_{lock} is approximately 4 MHz. Under these conditions, the long-term duration of the laser lock is approximately one week.

At its minimum value, the Lamb dip width could be the natural linewidth of the $2^3S_1 \rightarrow 2^3P_2$ transition (1.6 MHz). However, a number of broadening effects inside the cell appear to be contributing to the measured width. Although the broadening effects are not fully understood, they allow for a wider Lamb dip ($\sim$40 MHz) and thus larger capture range. A capture range of this magnitude is appropriate for a long-term frequency lock of the laser.

3.4 Experimental setup of the 707-nm laser

The optical setup for locking the 707-nm laser is shown in figure 3.9. The 1083-nm laser beam (derived from the locked 1083-nm laser) excites a narrow velocity group centered at $v_z = 0$ to the 2^3P_2 state. The 707-nm laser excites these atoms to the upper 3^3S_1 state (refer to figure 2.3).

A glass wedge is used to pick-off a small portion of the 707-nm light so that it can be monitored by the wavemeter and directs another small portion of the 707-nm beam to the saturated absorption setup for locking its laser frequency. This

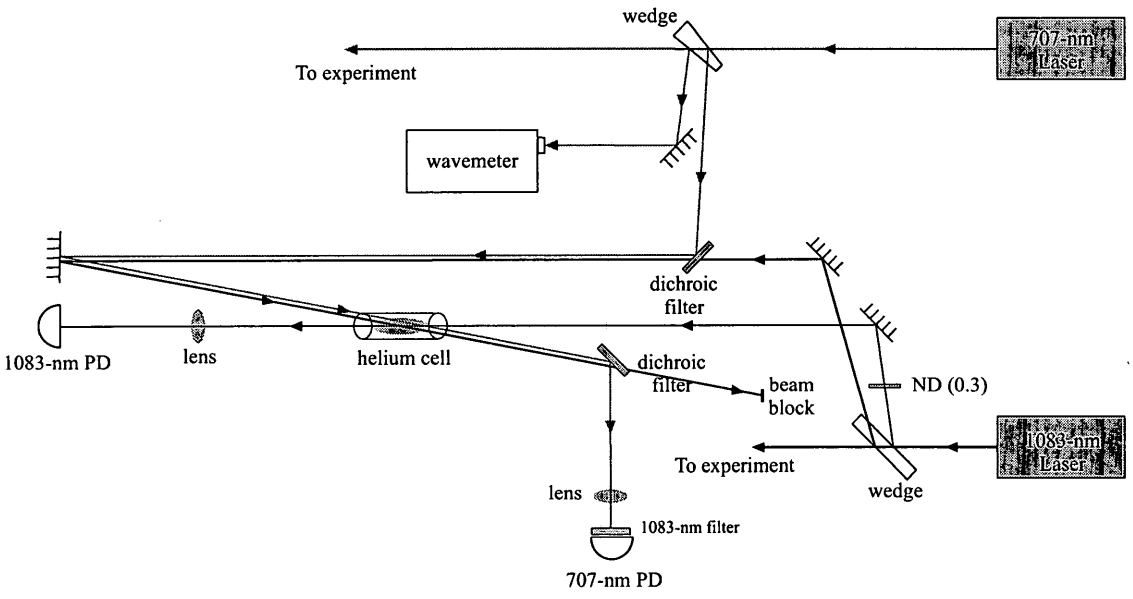

Figure 3.9: Experimental setup for 1083-nm and 707-nm laser systems. In this diagram, the 707-nm laser beam is offset from the 1083-nm pump beam for clarity. In the actual setup, the 707-nm beam overlaps the 1083-nm pump beam.

arrangement ensures that most of the 707-nm light is available for laser excitation of the atomic beam.

The 707-nm locking beam, which has a power of 150 μW and an intensity of 15 mW/cm^2, is overlapped with the 1083-nm pump using a dichroic filter positioned at 45° with respect to the incoming laser beams. The filter reflects 707-nm light and transmits 1083-nm light, thus allowing both laser beams to propagate through the helium cell. After passage through the cell, a second dichroic filter is used to separate the 707-nm beam from the 1083-nm light. The 707-nm beam is focused to a spot size much smaller than the 31-mm^2 active area of an InGaAsP photodiode, and its power is measured by this photodiode, along with a Melles-Griot (Large Dynamic Range) current amplifier.

Figure 3.10(a) shows the Doppler-selected resonance for the $2^3P_2 \rightarrow 3^3S_1$ transition at 707 nm. This 707-nm resonant signal is obtained by applying a triangle-wave modulation with a peak-to-peak amplitude of 260 mV (or peak-to-peak frequency modulation of 340 MHz) to the PZT control. Based on the 1.3 MHz/mV calibration, the width of the Doppler-selected resonance is inferred to be approximately 80 MHz (much larger than the 3.6 MHz natural linewidth for this transition). The 707-nm absorption width of figure 3.10(a) is dominated by the velocity class selected by the 1083-nm laser. The 40 MHz width of the velocity class selected by the 1083-nm beam implies a width for the 707-nm transition of 60 MHz (inferred

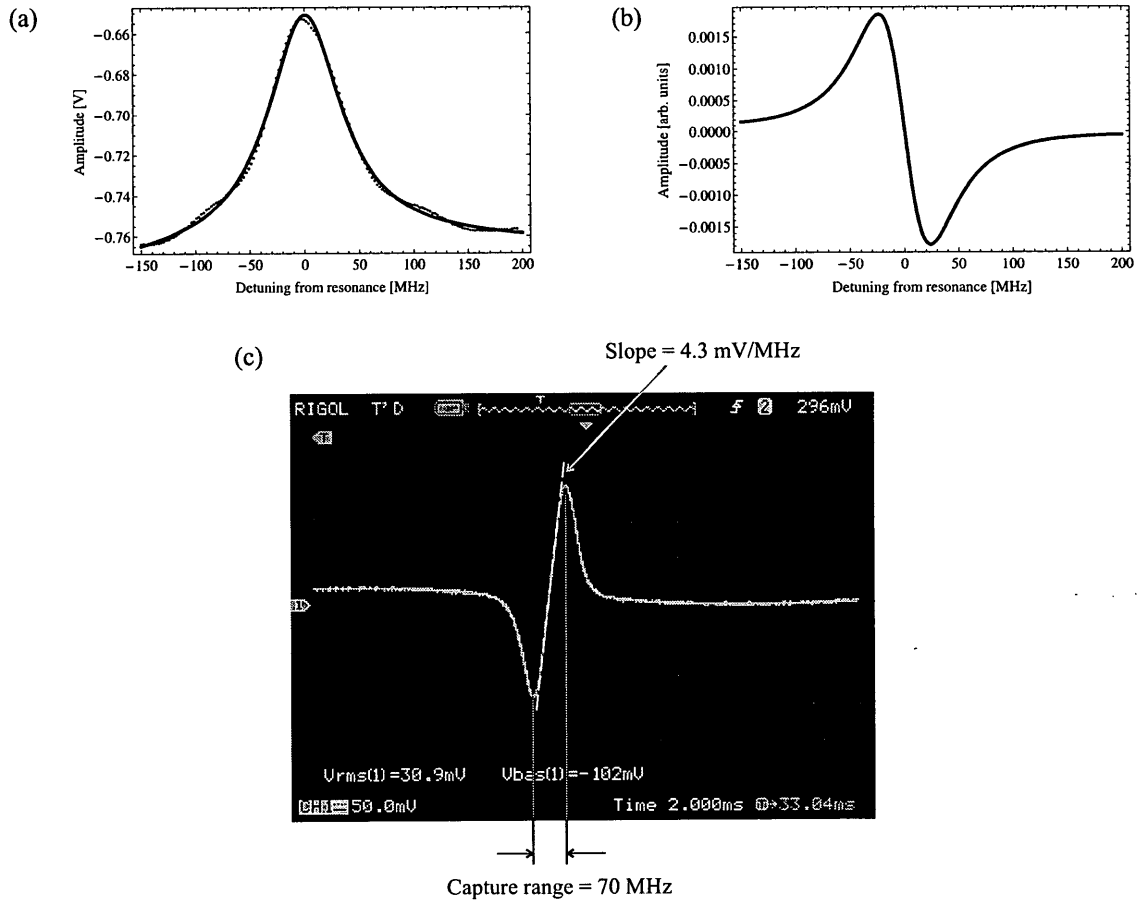

Figure 3.10: Locking signals for the 707-nm saturated absorption technique. (a) Doppler-selected resonance of the $2^3P_2 \rightarrow 3^3S_1$ transition. (b) Dispersion curve generated by the lock-in amplifier corresponding to the first derivative of the $2^3P_2 \rightarrow 3^3S_1$ absorption feature. (c) Oscilloscope trace of a 707-nm dispersion curve.

from the ratio of the 1083-nm and 707-nm wavelengths multiplied by the 40 MHz width of the 1083-nm transition). The observed 707-nm width is broadened to 80 MHz by a number of broadening processes, including power broadening, pressure broadening, and angle broadening (which results from Doppler broadening due to imperfect alignment of the two laser beams).

The derivative of the curve of figure 3.10(a) is shown in figure 3.10(b). It forms a dispersion curve appropriate for locking the frequency of the laser. This derivative curve can approximately be obtained by applying a small-amplitude frequency oscillation and finding the resulting first harmonic with a lock-in amplifier. The 30 MHz peak-to-peak oscillation is generated by a 25 mV triangle-wave (using the function generator of figure 3.11), and the lock-in amplifier is a EG&G Princeton Applied Research, Model 128A. Figure 3.10(c) shows the dispersion curve obtained in this way, which has a wider capture range (70 MHz) than the 50-MHz range of the derivative curve in part (b). A larger capture range is expected because the 30-MHz modulation waveform is too large to obtain the exact derivative curve of figure 3.10(b). The slope of the dispersion curve is 4.3 mV/MHz, as shown in figure 3.10(c).

The lock-in amplifier filters its output through an internal low-pass filter of 3 Hz, and this filtered output serves as the error signal for locking the laser frequency. The filtered lock-in output signal is sent through an ADC input of a LabJack U3,

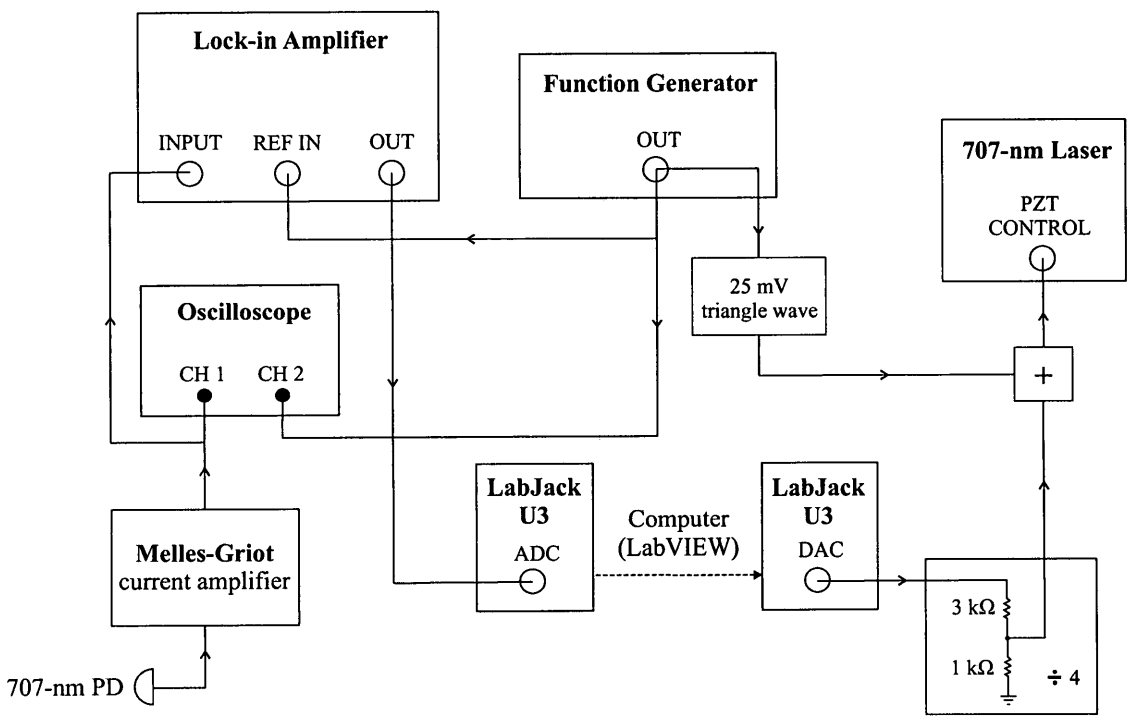

Figure 3.11: Feedback loop of the 707-nm locking system.

and to a LabVIEW program similar to the one used for the 1083-nm laser lock. In this case, the LSB value of 1.2 mV of the ADC corresponds to a frequency of 0.3 MHz. The program averages 50 error voltage readings every second and plots the averaged values as a function of time. The correction voltage is computed on the basis of this average and the proportional gain parameter, which is typically set to 0.4. Again, the value for the proportional gain is approximately the reciprocal of the slope of the dispersion curve (4.3 mV/MHz) and the laser frequency tuning factor after the factor-of-4 voltage divider of figure 3.11 (1.3/4 MHz/mV). The tolerance level is set to 13 mV (or a frequency of 3 MHz). This level gives the best laser lock, and lower tolerance levels do not show improvements in the lock stability. The output correction voltage from the DAC output of the LabJack U3 passes through a factor-of-4 voltage divider to internally adjust the laser frequency based on the feed-forward setting. The divided voltage correction for the LSB of the DAC is 1 mV, corresponding to 1.6-MHz corrections to the laser frequency. The 5-V tuning range of the DAC corresponds to a frequency range of 1.6 GHz. Like the 1083-nm feedback loop, the LabVIEW program applies corrections to the 707-nm laser once every second.

3.5 Results of the 707-nm laser

Studies of the lock stability using the standard deviation of the error voltage averages and the 4.3 mV/MHz slope of the dispersion curve show that σ_{lock} is approximately 6 MHz, based on measurements of laser locks of a few hours. The typical durations for the 707-nm laser lock is approximately 3 days.

The helium precision measurement requires σ_{lock} for both the 1083-nm and 707-nm lasers to be significantly reduced for laser cooling, optical pumping, and optimizing stability in signal detection. In an attempt to reduce σ_{lock}, the DAVLL scheme is used, as described in the next chapter. This scheme also offers the possibility of achieving a larger capture range, which could lead to a longer-duration lock.

4 Dichroic atomic vapour laser lock (DAVLL)

In this chapter the physical principles of the DAVLL technique are introduced. This is followed by a description of the DAVLL locking setup for the 1083-nm laser. The chapter concludes with a brief overview of the results obtained using this technique.

4.1 Introduction to DAVLL

The dichroic atomic vapour laser locking (DAVLL) technique [Corwin et al. (1998)] has a much larger capture range than the saturated absorption locking technique described in chapter 3. The DAVLL method relies on differential absorption between circularly polarized components of a laser beam passing through a reference cell within a uniform magnetic field. The applied magnetic field splits the Zeeman sublevels of a Doppler broadened transition.

The physical principle of the DAVLL technique can be illustrated using the experimental setup in figure 4.1. A linearly polarized laser beam is aligned through a vapour cell placed in a uniform magnetic field. The linearly polarized laser beam

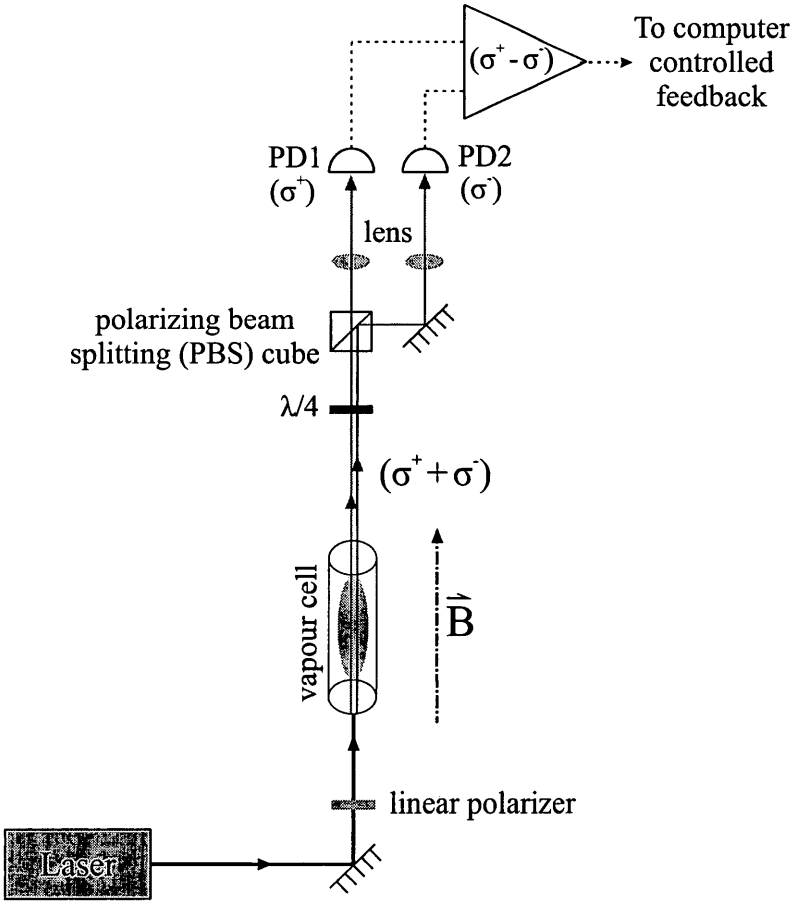

Figure 4.1: Experimental layout for the DAVLL locking technique.

consists of two equal components of right and left circular polarizations (σ^+ and σ^-). A quarter-waveplate ($\lambda/4$) and polarizing beam splitting (PBS) cube placed after the cell (see figure 4.1) can be used to separate the absorption signals associated with the two circularly polarized components. The absorption signals are detected on two photodiodes and subtracted electronically.

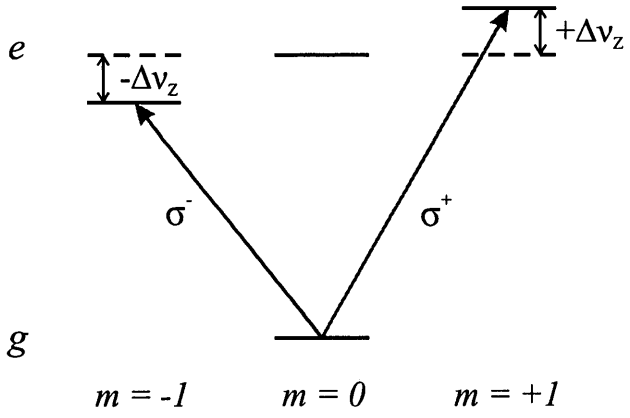

Figure 4.2: DAVLL for a simple-case atomic structure. Shown is the energy-level diagram for an atom with a simple electronic structure. The ground and excited states are denoted by g and e, respectively. The Zeeman shifts of the excited-states magnetic sublevels $\Delta\nu_z$ result from an applied magnetic field.

To illustrate the physical principle of DAVLL, we consider an atom with a simple electronic structure for the ground and excited states, as shown in figure 4.2. The $m = \pm 1$ sublevels of the excited state have equal and opposite Zeeman shifts, given by

$$\Delta\nu_Z = \pm\frac{g\mu_B mB}{h}, \tag{4.1}$$

where g is the Lande g-factor, μ_B is the Bohr magneton, m is the magnetic quantum number, and B is the applied magnetic field. The central curve (solid line) in figure 4.3(a) shows the Doppler-broadened spectral line in the absence of a magnetic field for the atomic system in figure 4.2. In the presence of a magnetic field, the absorption profiles for the Zeeman-shifted σ^+ and σ^- components of the laser beam are shown as dashed lines. The difference between these two components is negative below resonance and positive above resonance, as shown in figure 4.3(b). Therefore, the difference between the photodiode signals generates a dispersion shape with a zero-crossing at the atomic resonance frequency, and can thus be used for frequency stabilization of a laser. The slope of the dispersion-shaped error signal depends on the applied magnetic field. The strength of the B field is usually chosen such that the frequency difference between the two absorption peaks is on the order of the Doppler width, $\Delta\nu_D$, as shown in figure 4.3(a). The capture range (the frequency range between the turning points of the dispersion signal) is thus substantially larger than that for the saturated absorption technique.

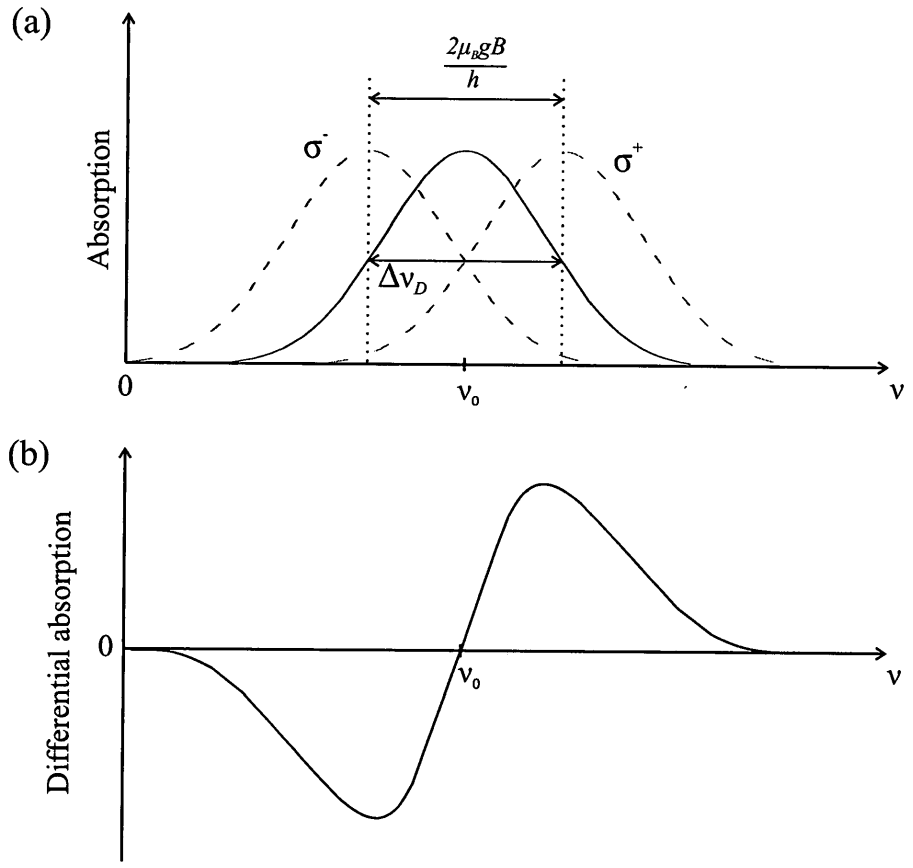

Figure 4.3: Origin of the DAVLL dispersion signal. (a) Zeeman shifts of the σ^+ and σ^- components of the absorption signal. (b) Dispersion profile produced by the difference between the σ^+ and σ^- absorption.

4.2 Experimental setup of the DAVLL lock for the 1083-nm laser

The 1083-nm laser beam for the DAVLL setup passes through a Faraday isolator to prevent optical feedback into the laser cavity (see figure 4.4). The light then passes through a half-waveplate ($\lambda/2$) and a PBS cube. These two elements constitute a variable beam-splitter. The linearly-polarized component transmitted by the PBS cube is used for the DAVLL lock, while the reflected component is available for the helium experiment.

The laser beam used for the DAVLL lock (with a power of 1 mW and an intensity of $\sim$50 mW/cm^2) passes through the helium cell, which is immersed in a magnetic field. The B field is created by a large solenoid (40 turns/cm) made of insulated magnet wire connected to a GW-INSTEK (GPS-1850D) DC power supply. The vapour cell is placed at the center of the solenoid, where the field is most uniform. After the cell, the laser beam passes through a quarter-waveplate and a PBS cube. This combination splits the light into its σ^+ and σ^- components. These σ^+ and σ^- components of the beam are focused and detected on two separate Melles-Griot silicon photodiodes (13 DSI 009), each with an active area of 31 mm^2. Again, the focused spot size of the two beams (σ^+ and σ^-) is much smaller than the active area of the photodiodes. The difference between these photodiode signals is analyzed

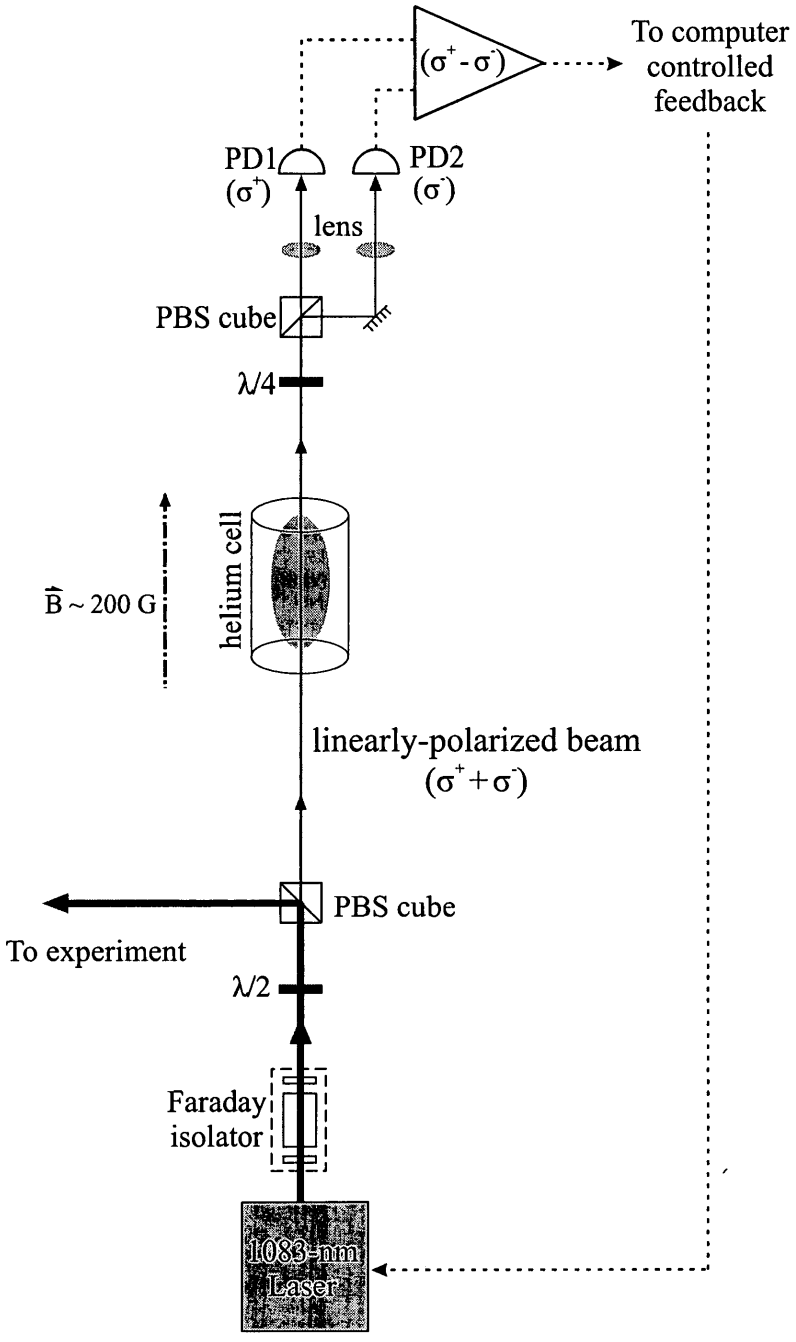

Figure 4.4: DAVLL experimental setup for the 1083-nm locking scheme.

using the subtraction circuit shown in figure 4.5, which, together with a Melles-Griot (Large Dynamic Range) current amplifier, produces a voltage proportional to the difference of the currents produced by the two photodiodes. Table 4.1 shows the Zeeman shift rates for the relevant helium energy levels [Borbely (2009)], and table 4.2 shows the resulting Zeeman shift rates for the σ^+ and σ^- laser transitions. Based on these rates, a B field of $\sim$200 G is chosen such that the frequency difference between the σ^+ and σ^- components of the 1083-nm $2^3S_1 \rightarrow 2^3P_2$ transition is $\sim$800 MHz.

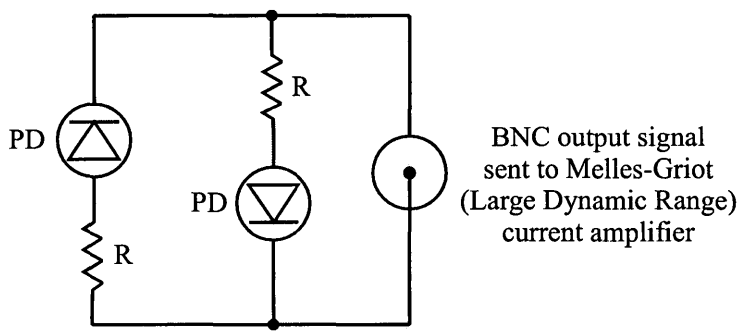

Figure 4.5: Circuit diagram of the subtraction detector. Here, R = 50 Ω.

To balance the σ^+ and σ^- powers, the magnetic field is first shut off, so that with the laser tuned far from resonance, the signals on the two photodiodes should be identical. If there is an offset detected by the subtraction circuit (figure 4.5), the quarter-waveplate is rotated until the difference between the σ^+ and σ^- signals is zero. Then the B field is turned on, and the laser frequency is scanned across resonance using an Agilent 33120A function generator connected to the current-

Table 4.1: Zeeman shifts of energy levels associated with the 2^3S_1, 2^3P_2, and 3^3S_1 states.

State	m-sublevel	Energy shift [MHz/G]
	m = -1	-2.8
2^3S_1	m = 0	0
	m = +1	+2.8
	m = -2	-4.2
	m = -1	-2.1
2^3P_2	m = 0	0
	m = +1	+2.1
	m = +2	+4.2
	m = -1	-2.8
3^3S_1	m = 0	0
	m = +1	+2.8

Table 4.2: Zeeman shifts of the 1083-nm and 707-nm transitions induced by circularly-polarized light.

Polarization	Transition	Energy difference [MHz/G]
σ^+	$2^3S_1(m=-1) \rightarrow 2^3P_2(m=0)$	+2.8
	$2^3S_1(m=0) \rightarrow 2^3P_2(m=+1)$	+2.1
	$2^3S_1(m=+1) \rightarrow 2^3P_2(m=+2)$	+1.4
σ^-	$2^3S_1(m=-1) \rightarrow 2^3P_2(m=-2)$	-1.4
	$2^3S_1(m=0) \rightarrow 2^3P_2(m=-1)$	-2.1
	$2^3S_1(m=+1) \rightarrow 2^3P_2(m=0)$	-2.8
σ^+	$2^3P_2(m=-2) \rightarrow 3^3S_1(m=-1)$	+1.4
	$2^3P_2(m=-1) \rightarrow 3^3S_1(m=0)$	+2.1
	$2^3P_2(m=0) \rightarrow 3^3S_1(m=+1)$	+2.8
σ^-	$2^3P_2(m=0) \rightarrow 3^3S_1(m=-1)$	-2.8
	$2^3P_2(m=+1) \rightarrow 3^3S_1(m=0)$	-2.1
	$2^3P_2(m=+2) \rightarrow 3^3S_1(m=+1)$	-1.4

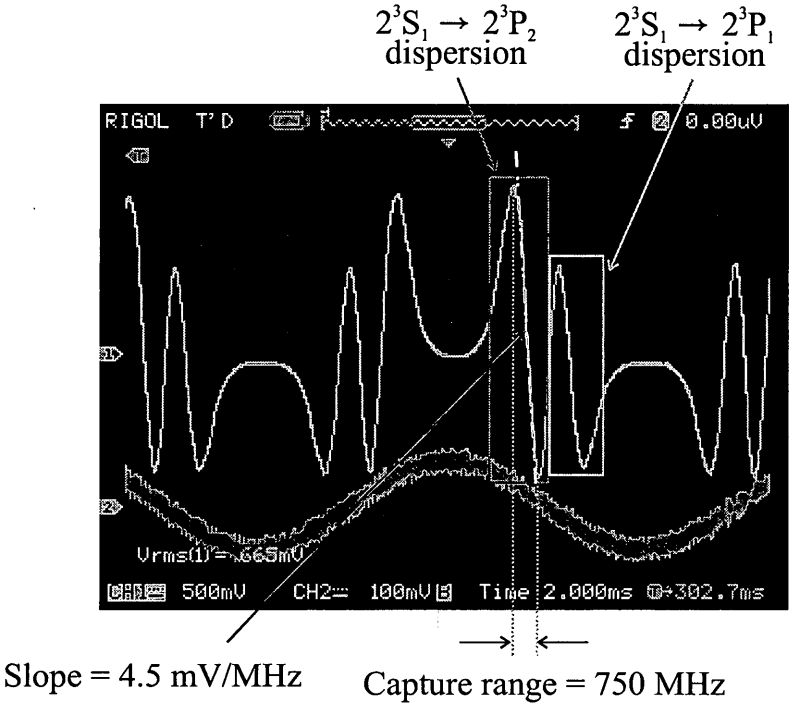

Figure 4.6: Oscilloscope trace of the 1083-nm DAVLL error signal.

adjust input of the laser controller (figure 4.6). The resulting dispersion signal is similar to that of figure 4.3(b). The zero-crossing of this dispersion signal should be at the atomic resonance. The oscilloscope trace of figure 4.6 shows dispersion curves for the $2^3S_1 \rightarrow 2^3P_2$ and $2^3S_1 \rightarrow 2^3P_1$ transitions. For this trace, the laser is scanned by a sinusoidal waveform set at a frequency of 143 Hz and a peak-to-peak amplitude of 180 mV (corresponding to approximately 7 GHz of peak-to-peak frequency modulation). A ~750 MHz capture range and a 4.5 mV/MHz slope can be inferred for the $2^3S_1 \rightarrow 2^3P_2$ transition (as shown in figure 4.6).

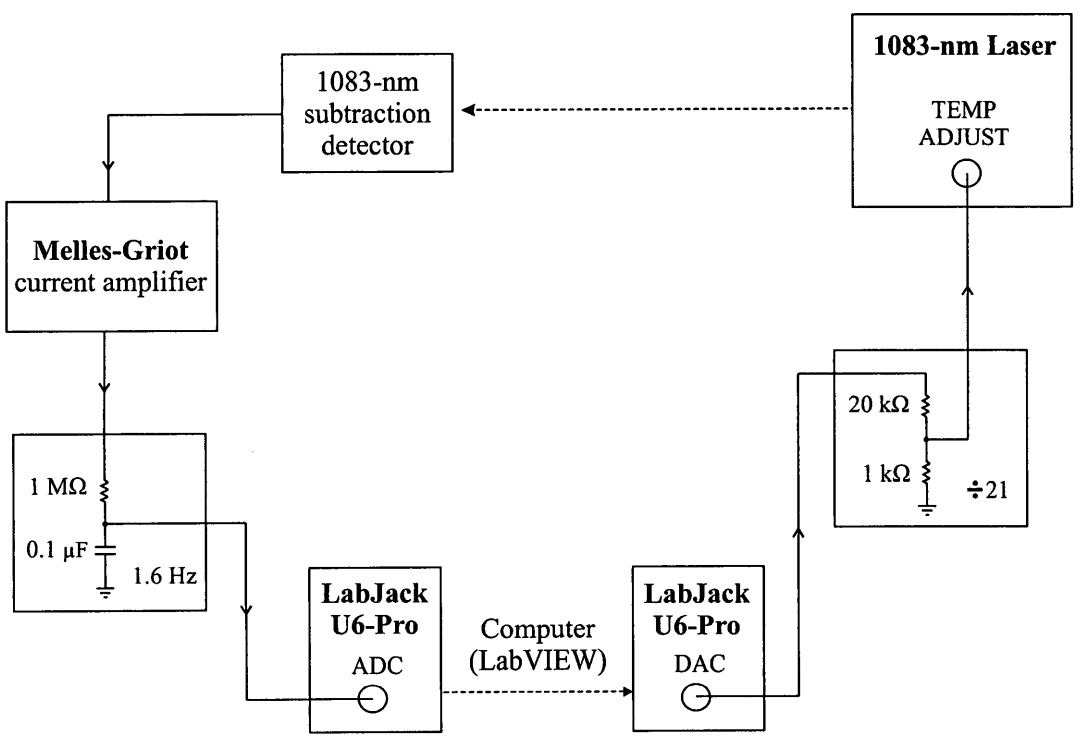

Figure 4.7: Feedback loop of the 1083-nm DAVLL setup.

Before engaging the laser lock, the modulation to the laser frequency is turned off. The current amplifier output signal of the subtraction circuit of figure 4.5 passes through a 1.6-Hz low-pass filter placed at the ADC input of a LabJack U6-Pro (as shown in figure 4.7). For this LabJack model, the input channels have a resolution of 18 bits and a range of ± 10 V, meaning that the LSB of the ADC has a voltage of 80 μV (corresponding to a frequency of approximately 20 kHz). As described in chapter 2, 50 error voltage readings from the LabJack are averaged in the LabVIEW program every second. Based on these averaged readings, the program plots the error signal as a function of time and computes the required correction voltage. The magnitude of the correction is the proportional gain parameter (typically 0.3) times the error voltage, and is applied only if the error voltage is outside of the tolerance level (set at 3 mV or a frequency of $\sim$700 kHz). Once again, the gain parameter is approximately the reciprocal of the product of the slope of the dispersion curve (4.5 mV/MHz) and the temperature-adjust tuning factor divided by a factor-of-21 voltage divider (19/21 MHz/mV). The laser lock stability shows no improvement for tolerance levels below the 3-mV setting. The correction voltage computed in software is sent to the DAC of the LabJack, which has a resolution of 12 bits and a range of 5 V. The DAC output correction voltage goes through the factor-of-21 voltage divider into the temperature-adjust input of the laser controller. The voltage-divided LSB value of the DAC is 60 μV, which corresponds to a frequency

of 1 MHz. In this case, the full 5-V tuning range of the DAC corresponds to a frequency range of 4.5 GHz. The error signal standard deviation is computed from a large number of points, where each point represents 50 error voltages averaged over one second. This standard deviation is converted from volts to frequency units using the slope of the dispersion curve (4.5 mV/MHz), and is used to infer the stability of the laser lock.

4.3 Results

The large capture range obtained from the DAVLL technique extends the duration of the lock to more than two weeks. The value for σ_{lock} of 1.3 MHz (see figure 4.8) is inferred from the standard deviation of the 1-s error voltage averages divided by the 4.5 mV/MHz slope of the dispersion curve. This σ_{lock} value is reduced by nearly a factor of 3 compared to the saturated absorption technique.

A disadvantage of the DAVLL technique is that the 2.29-GHz separation between the 2^3P_2 and 2^3P_1 energy levels is nearly the same order of magnitude as the 1.3 GHz Doppler-broadened linewidth (see figure 4.6). The Doppler-broadened linewidth leads to an offset in the zero-crossing of the $2^3S_1 \rightarrow 2^3P_2$ dispersion curve due to overlap with the neighbouring $2^3S_1 \rightarrow 2^3P_1$ dispersion curve. Additionally, fluctuations in the beam polarization associated with the zero-order quarter-waveplate cause drifts in the induced offset of the $2^3S_1 \rightarrow 2^3P_2$ dispersion curve.

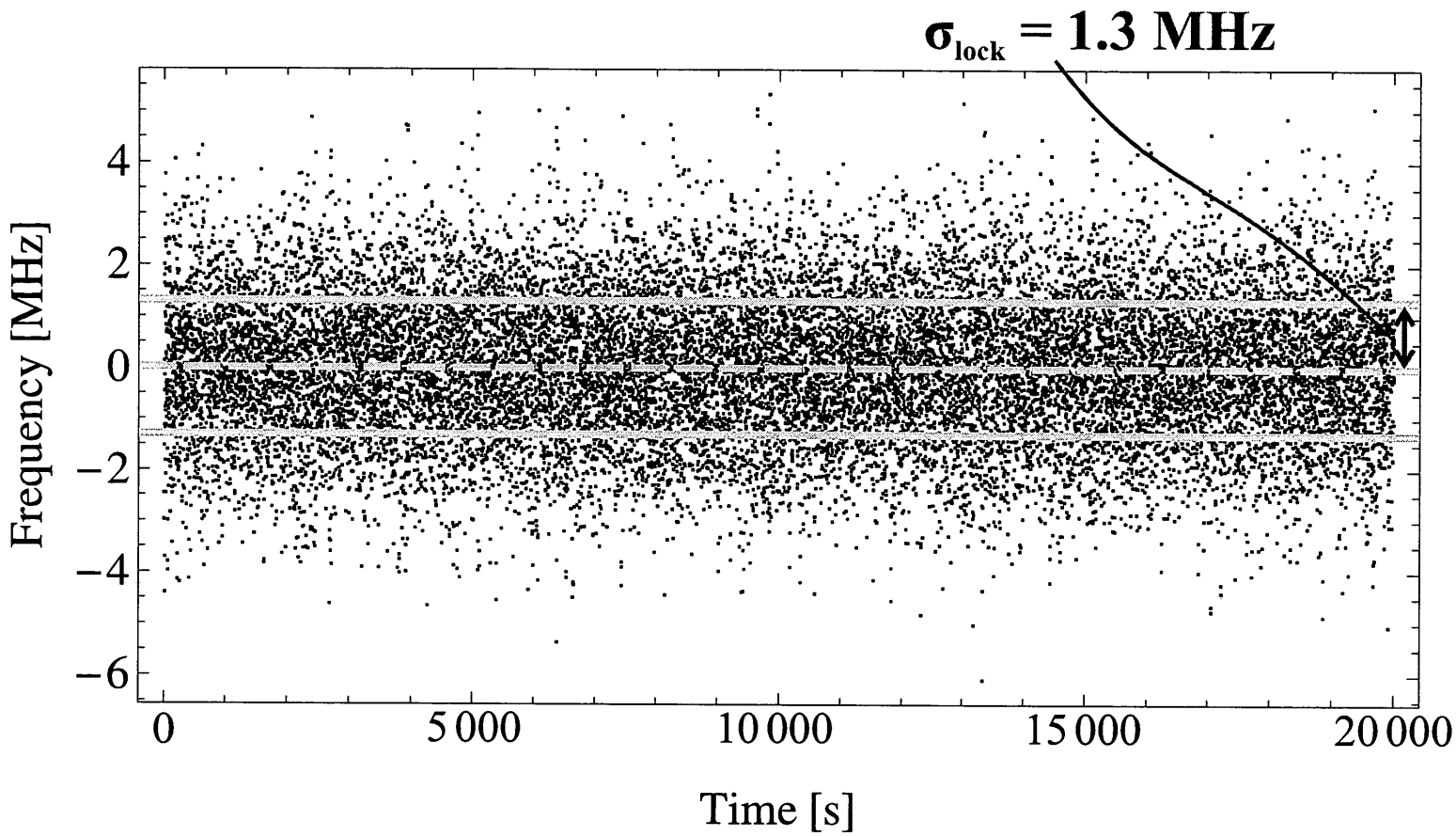

Figure 4.8: Locked DAVLL error signal for the 1083-nm laser. Each data point in the plot is inferred from the average of 50 error voltage LabJack readings (or a 1-s average). Shown are 20 000 s of data, which represents only a small fraction of the longer than 2 weeks of lock possible with this locking technique.

Such changes in the beam polarization are possibly the result of ambient temperature fluctuations that affect the birefringence of the waveplate. These polarization fluctuations can cause a drift in the zero-crossing of the dispersion curve and thus the lock point for the laser, thus causing frequency drifts in addition to the 1.3-MHz frequency fluctuations of figure 4.8.

4.4 DAVLL technique for locking the 707-nm laser

The intensity of the helium discharge in the vapour cell suggested that electron-impact excitation might directly populate the 2^3P_2 level without requiring optical excitation with the 1083-nm laser. However, an attempt to obtain a DAVLL signal for the 707-nm transition without the use of the 1083-nm laser did not prove successful. Due to the relatively large σ_{lock} of the 1083-nm DAVLL signal, this locking method was not pursued further. Instead, an improved technique called DS-DAVLL was adopted, which became the main focus of the thesis. This technique is described in the next two chapters.

5 Doppler-selective-DAVLL (DS-DAVLL) for the 1083-nm laser

5.1 Introduction to DS-DAVLL

The DS-DAVLL (Doppler-selective-DAVLL) technique [Giannini et al. (2007)] combines the concept of saturated absorption spectroscopy and the DAVLL method. In a saturated absorption setup, atoms in a velocity group centered at $v_z = 0$ are selected by the pump laser beam and observed by a probe beam, thus creating a Lamb dip. If a magnetic field is applied to the helium reference cell in this setup, the $2^3S_1(m) \rightarrow 2^3P_2(m')$ transitions become non-degenerate, as shown in table 4.2. In this situation, the σ^+ and σ^- components of the probe laser beam give rise to Lamb dips that are Zeeman-shifted above and below the atomic resonance, as shown in figure 5.1(a). The differential absorption between the σ^+ and σ^- components, shown in figure 5.1(b), generates a dispersion signal which can be used to stabilize the laser frequency. Unlike the ~1-GHz wide Doppler-broadened DAVLL

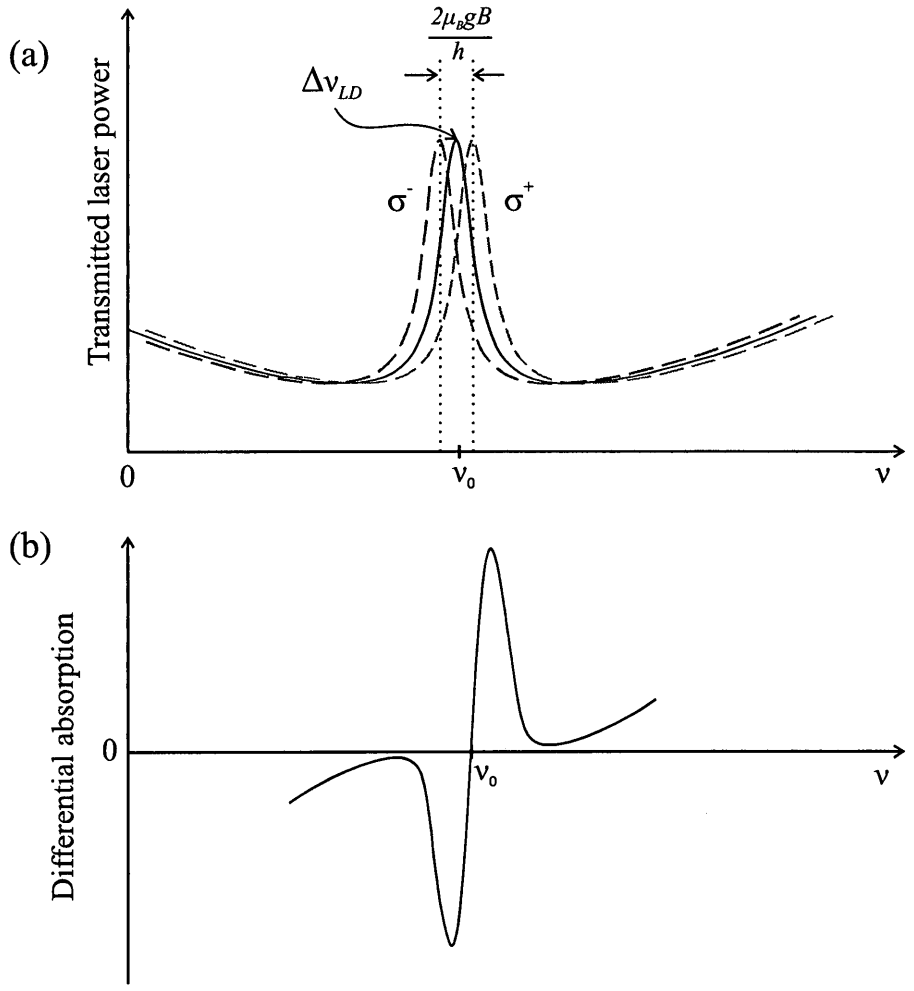

Figure 5.1: Origin of the DS-DAVLL dispersion signal. (a) The solid line represents a Lamb dip corresponding to the central region of figure 3.4 in chapter 3. The dashed lines show the Zeeman shifts of the σ^+ and σ^- components of the Lamb dip. (b) Dispersion profile produced by the difference between the σ^+ and σ^- components of (a).

dispersion curves, the DS-DAVLL signal has a much smaller capture range, which is approximately 40 MHz (the width of the Lamb dip). The narrowness of the Doppler-free lineshape requires a much smaller B field (~10 G, based on table 4.2) compared to the DAVLL technique.

The DS-DAVLL technique can lead to an improvement in the quality of the laser lock because the narrowing in the dispersion signal creates a steeper slope, and therefore a stronger signal for stabilizing the laser frequency. This locking technique is shown to reduce σ_{lock}, but at the expense of a reduced capture range.

5.2 Experimental setup

The experimental layout for the DS-DAVLL technique is outlined in figure 5.2. After passing through a Faraday isolator, most of the 1083-nm laser light is selected for the helium experiment using a variable beam splitter. The remaining 1083-nm laser light passes through a half-waveplate and a PBS cube creating two linearly polarized beams with variable intensities. The weak transmitted component (with a power of 3 mW and an intensity of ~150 mW/cm^2) is chosen as the probe beam, while the more intense reflected component (with a power of 10 mW and an intensity of ~500 mW/cm^2) is used as the pump beam. The pump and probe beams counter-propagate inside a helium reference cell in a typical saturated absorption setup. The only change required to modify the saturated absorption setup into a

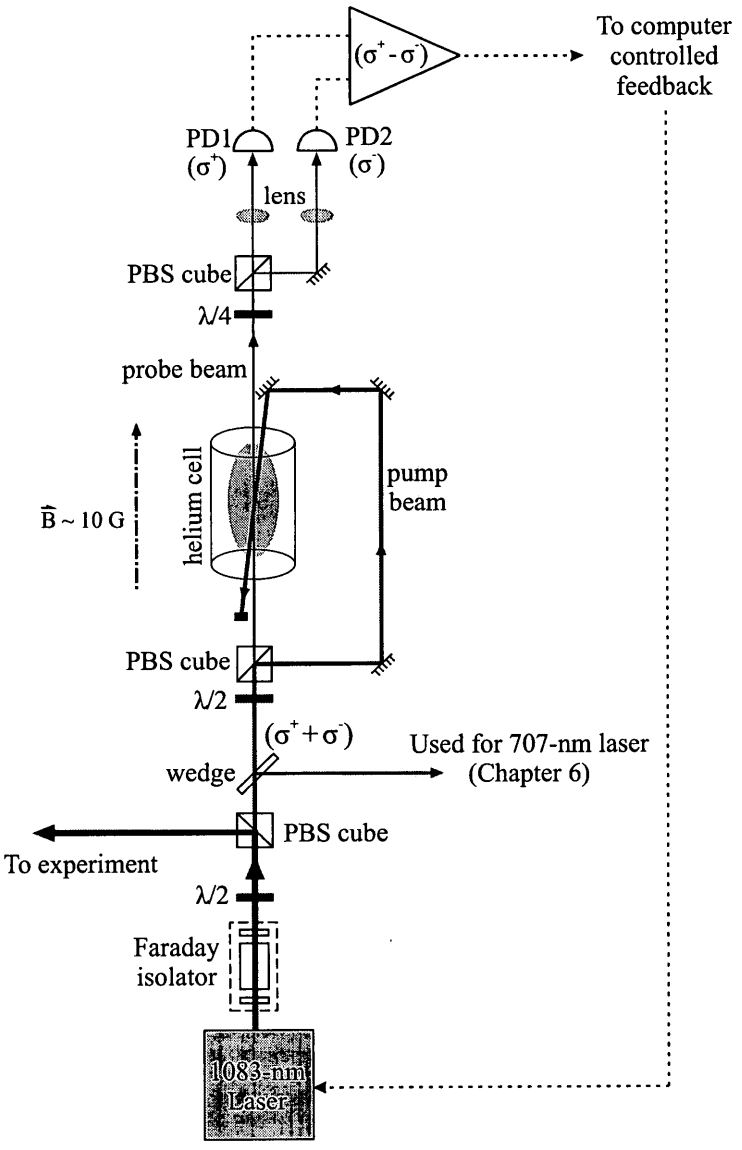

Figure 5.2: DS-DAVLL experimental setup for the 1083-nm laser. The angle between the pump and probe beam is exaggerated for clarity. In the actual setup, the pump and probe beams are within 10 mrad of anti-parallel with respect to each other.

DS-DAVLL setup is the placement of Helmholtz coils (with a diameter of 17 cm) around the helium cell. The coils are powered by a GW-INSTEK (GPS-1850D) DC power supply to produce a nearly uniform 10-G field. After passage through the cell, the pump beam is sent to a beam dump, while the counter-propagating probe beam passes through a quarter-waveplate and a PBS cube which separates out the σ^+ and σ^- components of the laser beam. The σ^+ and σ^- beams are focused onto two separate Melles-Griot silicon photodiodes (13 DSI 009) which have an active area of 31 mm^2. As in the DAVLL technique, the differential absorption between the σ^+ and σ^- components can be measured using the subtraction detector (figure 4.5). The subtracted signal passes through a Melles-Griot (Large Dynamic Range) current amplifier and a 1.6-Hz low-pass filter.

In order to observe the dispersion curve, the 1083-nm laser frequency can be scanned by a triangle waveform at a peak-to-peak amplitude of 100 MHz. The scan is created by an Agilent 33120A function generator, which supplies a triangle wave to the current-adjust input of the laser controller. The frequency scan produces a dispersion signal with a zero-crossing at the atomic resonance, as shown in figure 5.3. As expected, the capture range is approximately the width of the Doppler-free resonance, which is approximately 40 MHz. A straight-line fit in the vicinity of the zero-crossing displayed by the red line on the graph shows that the slope is 90 mV/MHz.

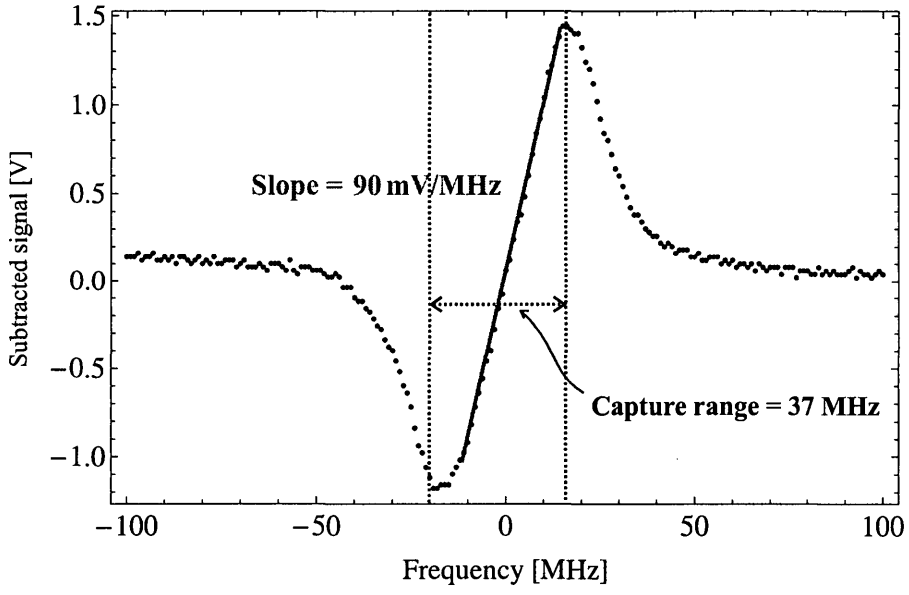

Figure 5.3: 1083-nm DS-DAVLL dispersion signal.

Once the frequency scan is disengaged and the laser is tuned near resonance, the laser lock can be enabled. Like the previous two techniques, the DS-DAVLL locking program averages 50 error voltage readings from the ADC of a LabJack U6-Pro, and outputs a correction voltage every second based on these 1-s averages. The LSB voltage of this ADC is approximately 80 μV, which corresponds to a frequency of 1 kHz. The voltage output goes through the DAC of the LabJack and a factor-of-470 voltage divider into the temperature-adjust of the laser (figure 5.4). The voltage-divided LSB value of the DAC is 2.5 μV, corresponding to a frequency of approximately 25 kHz. The full 5-V tuning range corresponds to a frequency range of 106 MHz. The corrections are applied only if the error signal

indicates that the laser frequency has drifted outside of the tolerance level (set at 3 mV, or a frequency of 35 kHz). Lower settings in the tolerance level do not lead to improvement in the laser stabilization. As in previous chapters, the proportional gain setting (typically 0.4) is approximately the reciprocal of slope of the dispersion curve (90 mV/MHz) multiplied with the temperature-adjust tuning parameter after the factor-of-470 voltage divider (10/470 MHz/mV).

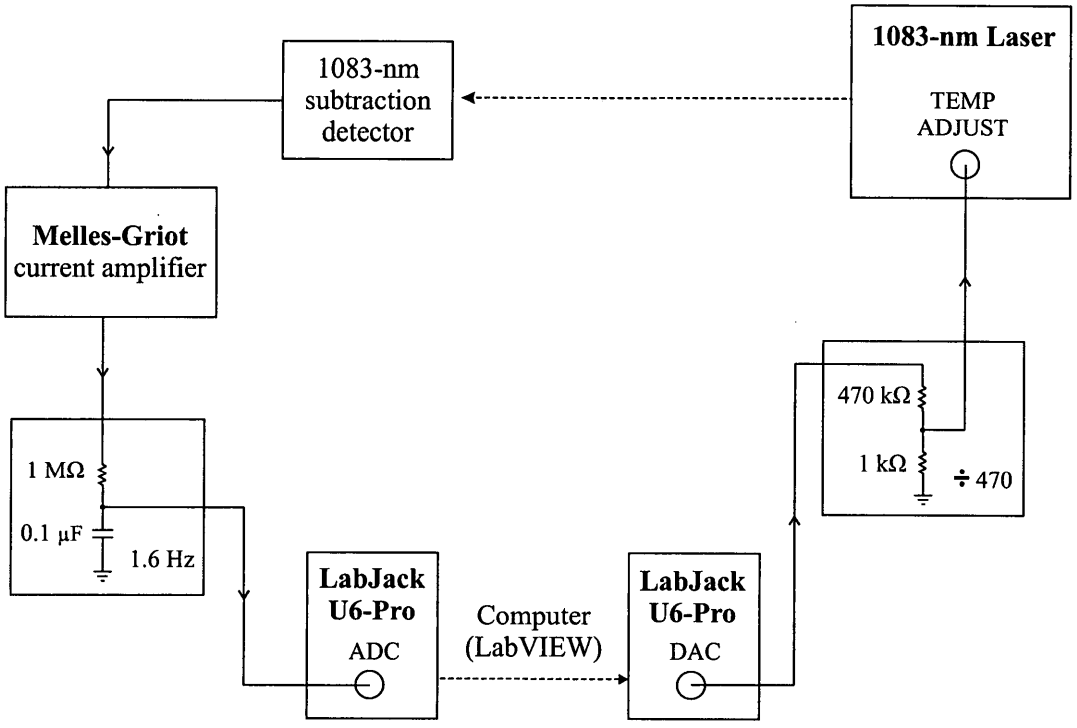

Figure 5.4: Feedback loop of the 1083-nm DS-DAVLL setup.

5.3 Results

The 90 mV/MHz slope obtained from the dispersion curve of figure 5.3 is much larger than the 4.5 mV/MHz slope associated with the DAVLL signal. As a result, it can be expected that the value of σ_{lock} is substantially reduced compared to the DAVLL technique. This expectation is supported by the data in figure 5.5, which shows σ_{lock} inferred from the standard deviation of the 1-s error voltages divided by the slope of the dispersion curve. For this technique, the value of σ_{lock} is 40 kHz, which is a significant reduction compared to the results of the previous chapters. Despite the smaller capture range, the laser remains locked for several weeks under these conditions. The data shown in figure 5.5 represents a small time frame compared to the typical duration of the lock. Based on the recorded DAC voltages during periods when the laser was locked, it can be inferred that an unlocked laser would exhibit frequency drifts ranging from about 2 to 15 MHz/day.

Our studies for the 1083-nm DS-DAVLL technique are successful in obtaining a suitably small σ_{lock} necessary for keeping the laser frequency locked on a time-scale of several weeks. The broadened Lamb dip provides a sufficient capture range for a long-term lock. The next chapter reviews similar results for the DS-DAVLL technique applied to the 707-nm laser.

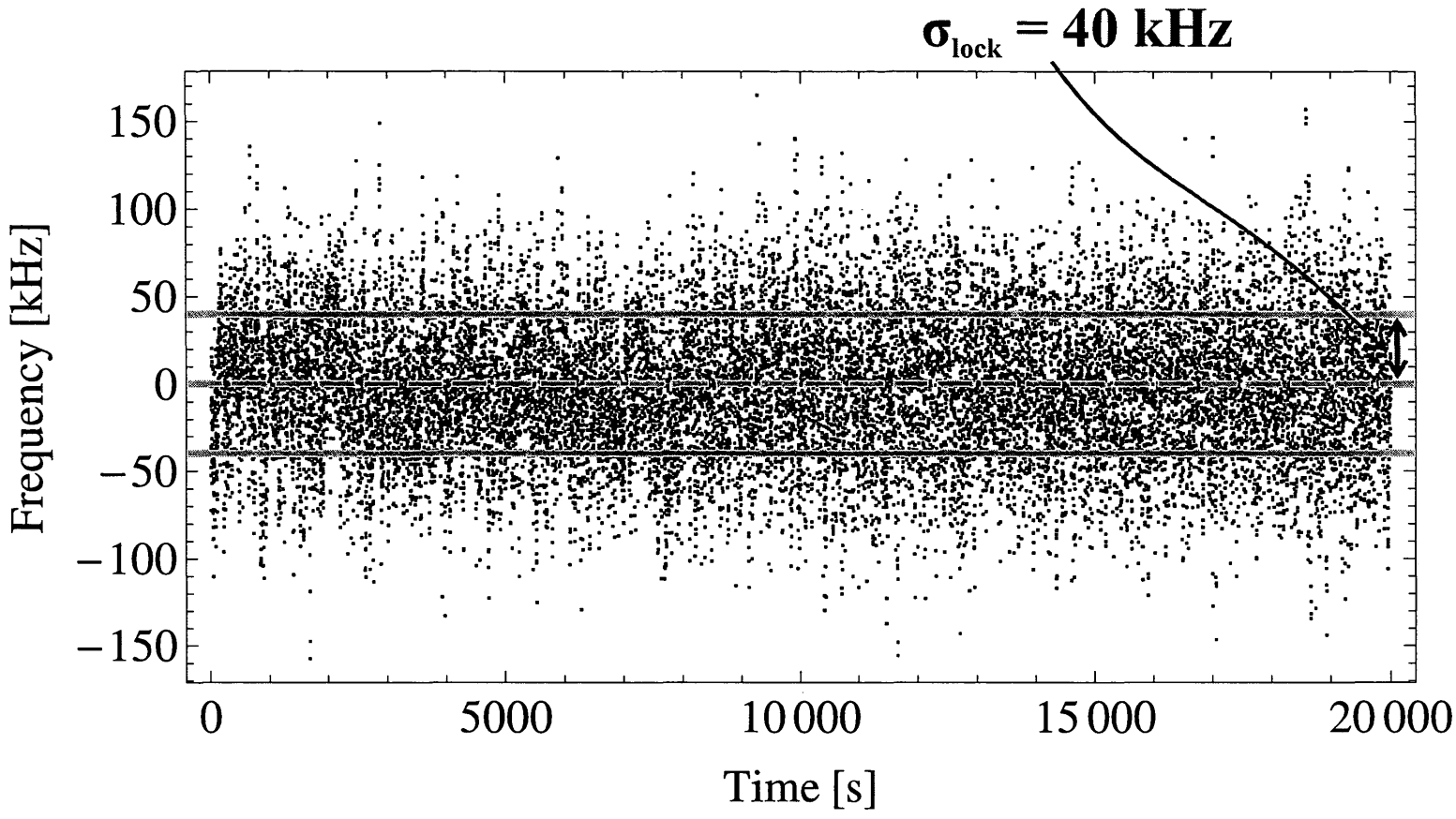

Figure 5.5: Locked DS-DAVLL error signal for the 1083-nm laser. Each point is derived from a 1-s average of the error voltage.

6 Doppler selective-DAVLL (DS-DAVLL) for the 707-nm laser

6.1 Application of DS-DAVLL to the 707-nm transition

To apply the DS-DAVLL technique to the 707-nm laser, a 1083-nm laser beam is overlapped with a 707-nm beam inside a reference cell to drive helium atoms from the 2^3P_2 state to the 3^3S_1 state. Since the 1083-nm laser is locked to the $v_z \sim 0$ velocity class, the 707-nm light can only excite atoms in this zero-velocity group to the 3^3S_1 state.

As in the case for the 1083-nm laser, a uniform magnetic field is applied to a second helium reference cell, to lift the degeneracy of the the $2^3P_2(m) \rightarrow 3^3S_1(m')$ transition (refer to table 4.2). Differential absorption in the resulting σ^+ and σ^- components gives rise to 707-nm absorption features that are shifted above and below resonance, respectively. Subtraction of these shifted resonances generates a dispersion signal (similar to figure 5.1(b)) with the zero-crossing occurring at the

707-nm atomic resonance. Based on such a dispersion signal, the 707-nm laser frequency can be locked in a similar manner to that of the 1083-nm laser. It is important to note that any fluctuations in the 1083-nm frequency are picked up by the 707-nm laser. This effect occurs because the two laser beams are overlapped inside the cell and the 707-nm laser can only interact with atoms that have populated the 2^3P_2 state through 1083-nm photon excitation.

6.2 Experimental setup

The DS-DAVLL experimental setup for the 707-nm laser is similar to that of the 1083-nm laser, as shown in figure 6.1. The 707-nm laser output is sent through a Faraday isolator to avoid optical feedback into the laser cavity. After passing through the isolator, a glass wedge sends a portion of the light to a wavemeter for monitoring the laser frequency, as described in chapter 2. A variable beam-splitter directs a portion of the beam to the DS-DAVLL setup. Most of the laser light reflects off the PBS cube so that it can be used for the helium experiment.

The 707-nm DS-DAVLL setup uses a helium discharge reference cell placed inside a pair of Helmholtz coils (with a diameter of 12 cm) connected to a current supply. The coils are used to generate a uniform magnetic field of approximately 20 G. A 1083-nm beam (with an intensity of $\sim$250 mW/cm^2 and power of 5 mW) is locked to the $2^3S_1 \rightarrow 2^3P_2$ resonance using a DS-DAVLL setup, as described in the

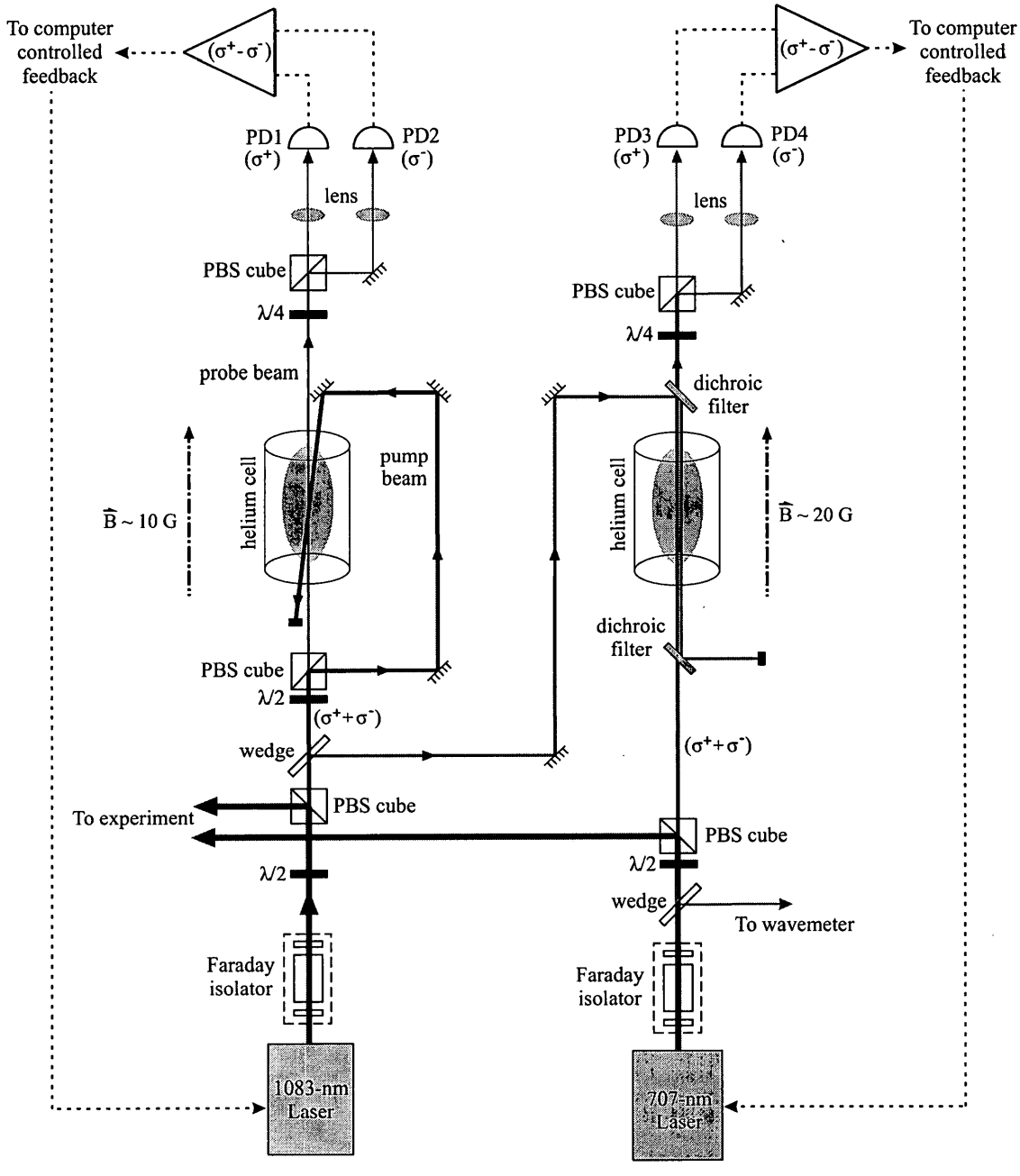

Figure 6.1: Experimental setup for the 707-nm DS-DAVLL system.

previous chapter. A portion of the beam from this setup passes through the helium cell of the 707-nm DS-DAVLL setup. Since the 707-nm light (with a power of 3 mW and an intensity of $\sim$150 mW/cm^2) is counter-propagated with the 1083-nm laser, the two lasers excite a narrow velocity class around $v_z \sim 0$ to the upper 3^3S_1 state. These are the atoms first excited by the 1083-nm laser to the $^3P_2$ state, as shown in figure 2.3, and the velocity class is defined by the 1083-nm laser linewidth.

Before passing through the reference cell in the 707-nm DS-DAVLL setup, the 1083-nm laser is overlapped with the 707-nm light using a dichroic filter. After passage through the cell, the 707-nm beam is separated from the 1083-nm beam using another dichroic filter. The 1083-nm then goes to a beam block, while the 707-nm beam passes through a quarter-waveplate and a PBS cube. Just like the DS-DAVLL setup for the 1083-nm laser, the σ^+ and σ^- components are focused onto two separate Melles-Griot silicon photodiodes (13 DSI 009), with an active area of 31 mm^2, inside a subtraction detector. Once again, the spot size of the σ^+ and σ^- beams is much smaller than the active area of the photodiodes. The subtracted signal is sent through a Melles-Griot (Large Dynamic Range) current amplifier and a 1.6-Hz low-pass filter.

The 707-nm laser frequency can be scanned across 1 GHz using a triangle wave sent to the PZT control input. This scan generates a dispersion error signal corresponding to the $2^3P_2 \rightarrow 3^3S_1$ transition, as shown in figure 6.2. The slope around

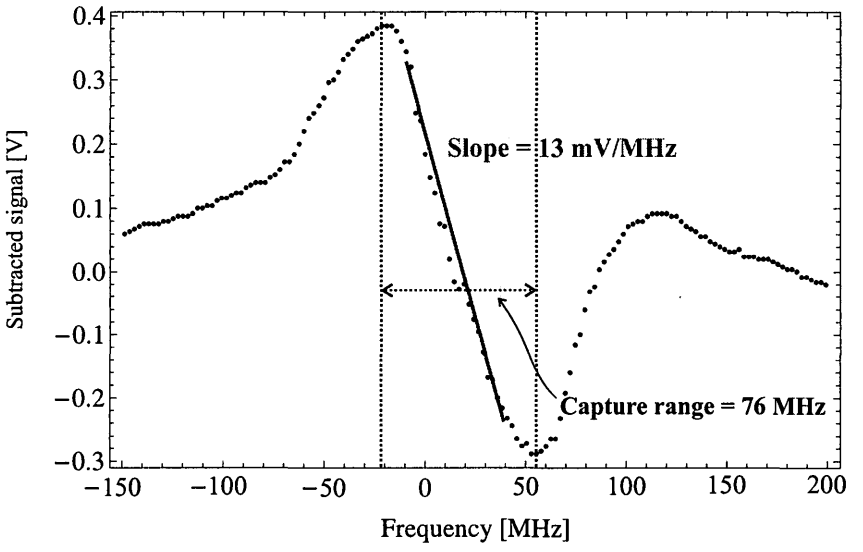

Figure 6.2: Dispersion-shaped error signal corresponding to the 707-nm DS-DAVLL system.

the zero-crossing is 13 mV/MHz.

To lock the lasers, the frequency scan is turned off. The current amplifier output signal goes to the ADC input of the LabJack U6-Pro (with a LSB voltage of 80 μV, corresponding to a frequency of 6 kHz) to the LabVIEW computer program for frequency locking (figure 6.3). The correction voltage computed in LabVIEW is sent to the DAC of the LabJack through a factor-of-48 voltage divider and into the PZT-control of the laser. The voltage-divided LSB voltage output is 25 μV, corresponding to a frequency of 32 kHz. Here, the 5-V tuning range of the DAC corresponds to a frequency range of 135 MHz. Just like the DS-DAVLL program for the 1083-nm laser, the 707-nm locking program averages 50 error voltages every

second and plots them as a function of time. The correction voltage from the LabVIEW program is applied every second, based on the proportional gain setting and tolerance level. The proportional gain (typically set at 1.8) is approximately the reciprocal of the slope of the dispersion curve (13 mV/MHz) multiplied with the factor-of-48 voltage-divided PZT-control tuning factor (1.3/48 MHz/mV). The tolerance level is set to 1 mV or a frequency of 80 kHz, and lower settings do not improve the laser lock.

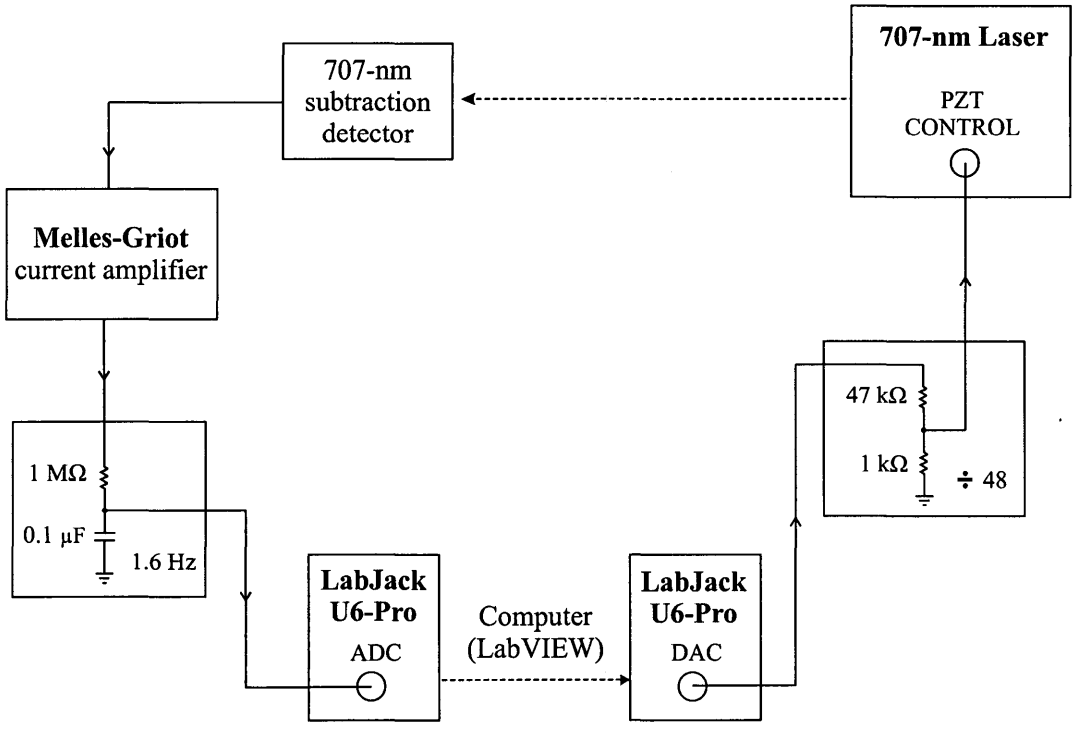

Figure 6.3: Feedback loop of the 707-nm DS-DAVLL setup.

6.3 Results

Figure 6.4 shows the value of σ_{lock} is 140 kHz, which is inferred from the standard deviation of 1-s error voltage averages divided by the 13 mV/MHz slope of the dispersion curve. The frequency excursions of this laser are approximately three times as large as the ones for the 1083-nm laser. Based on the recorded DAC voltages during periods when the laser was locked, it can be inferred that an unlocked laser would exhibit frequency drifts ranging from about 2 to 20 MHz/day.

Figure 6.5 shows the frequency drifts of the locked error signal of figure 6.4 on a much shorter time scale. The slow frequency drifts of the error signal suggest that an even tighter lock should be possible.

The 707-nm laser remains locked for time scales of several weeks. The capture range of the 707-nm dispersion curve (figure 6.2) is much larger than the natural linewidth (3.6 MHz) of the $2^3P_2 \rightarrow 3^3S_1$ transition, and this allows for a long-term laser frequency lock.

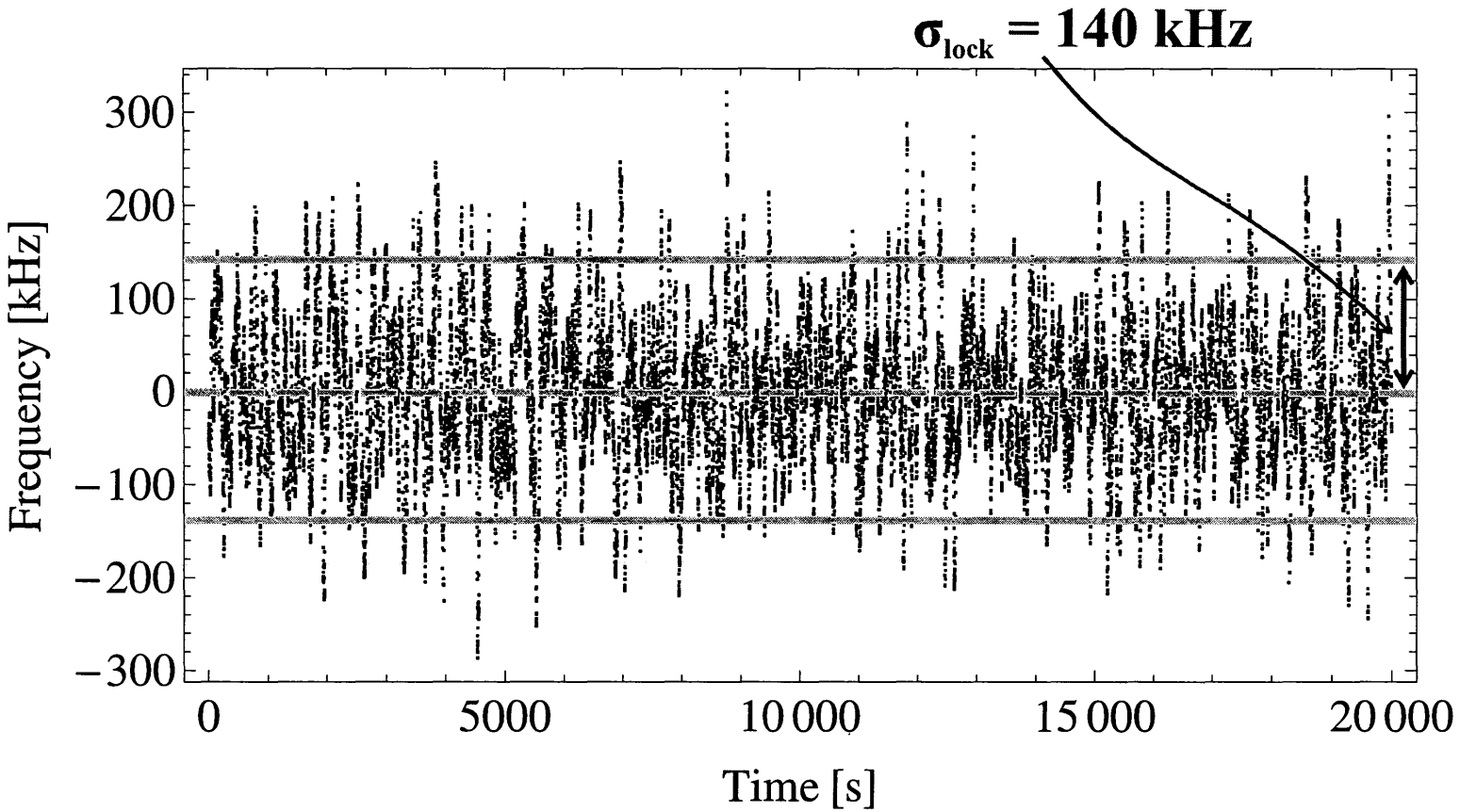

Figure 6.4: Locked DS-DAVLL error signal for the 707-nm laser. Each point is derived from a 1-s average of the error voltage.

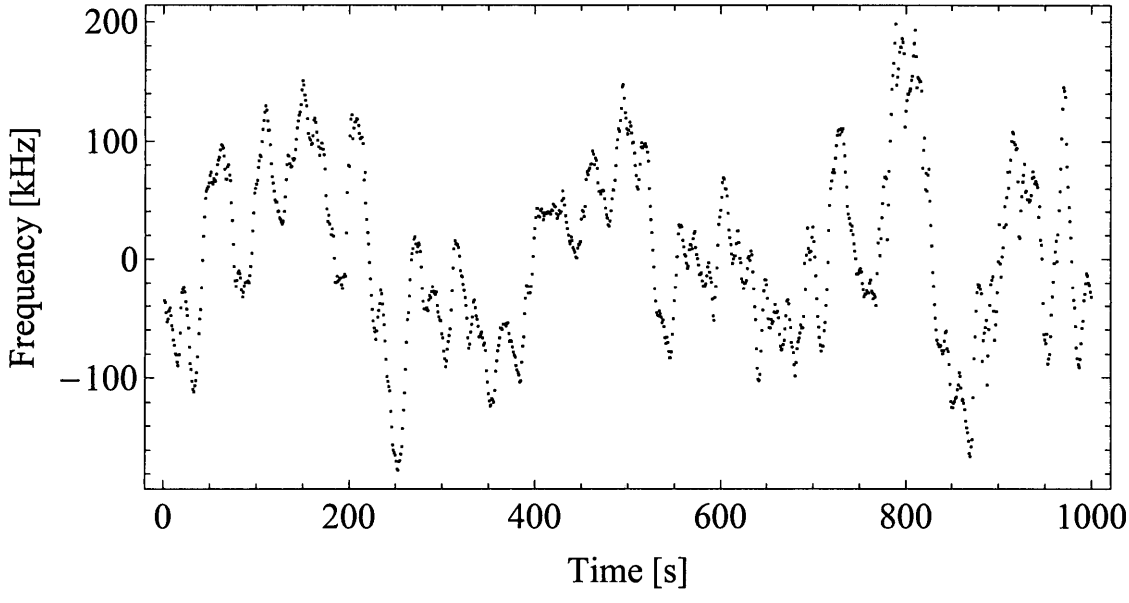

Figure 6.5: Short-term locked DS-DAVLL error signal for the 707-nm laser. The plot shows the first 1 000 seconds of the locked signal of figure 6.4.

7 Summary and future work

In this thesis, we have applied the DS-DAVLL technique to improve the value of σ_{lock} for the 1083-nm and 707-nm lasers to support precision measurements of atomic level structure in helium. We have achieved a σ_{lock} value of 40 kHz for the 1083-nm transition, and 140 kHz for the 707-nm transition, using the DS-DAVLL technique. This work also showed the comparative advantages of the DS-DAVLL technique over the standard saturated absorption technique and the DAVLL technique.

The main advantage of the DS-DAVLL technique is that the dispersion-shaped error signal can be generated using a relatively small magnetic field, without using a lock-in amplifier, and without laser frequency modulation. The application of the DAVLL technique to a Doppler-free resonance results in an increased slope of the dispersion signal and large enough capture range, to allow the 1083-nm laser to be locked for extensive periods of time. As a result, we have substantially advanced the goal of improving our laser frequency stability, and this increased stability will help for laser cooling the helium atomic beam and will result in a more stable detection

signal with a higher S:N ratio.

This work focused on stabilizing the laser on approximately a one-second time constant. The corrections to the laser frequency were made only once a second, and these corrections were based on the average of the error signal over the previous second. Since the 2^3P fine-structure measurements made by our group involve signals averaged over several seconds, the one-second average gives a good indication of the expected stability of our detection signal. However, to ensure highly efficient optical pumping and laser cooling, the lasers need to show stability on shorter time scales as well. Demonstrated stability on shorter time scales will be the subject of continuing research within our group. Since the time constant of the feedback loop of the 1083-nm laser was limited by the response time of the temperature adjust, further improvements might be achieved by dividing the error signal into high- and low-frequency components, with the high-frequency component fed back into the current adjust and the low-frequency component into the temperature adjust. A decrease in the Lamb dip width might also reduce σ_{lock} for the 1083-nm laser transition, but with a potential disadvantage of reducing the capture range.

The frequency locks achieved using the DS-DAVLL technique represent a significant improvement (approximately a factor of 50 in σ_{lock}) over our saturated absorption locks.

Bibliography

T. Aoyama, M. Hayakawa, T. Kinoshita, and M. Nio. Revised value of the eighth-order contribution to the electron $g-2$. *Phys. Rev. Lett.*, 99:110406, 2007.

T. Aoyama, M. Hayakawa, T. Kinoshita, and M. Nio. Tenth-order QED contribution to the electron $g-2$ and an improved value of the fine structure constant. *Phys. Rev. Lett.*, 109:111807, 2012.

J. S. Borbely. *Separated Oscillatory Field Microwave Measurement of the n=2 $^3P_1$ - n=2 $^3P_2$ Fine-Structure Interval of Helium.* PhD thesis, York University, 2009.

J. S. Borbely, M. C. George, L. D. Lombardi, M. Weel, D. W. Fitzakerley, and E. A. Hessels. Separated oscillatory-field microwave measurement of the $2^3P_1 - 2^3P_2$ fine-structure interval of atomic helium. *Phys. Rev. A*, 79:060503, 2009.

K. L. Corwin, Z. T. Lu, C. F. Hand, R. J. Epstein, and C. E. Wieman. Frequency-stabilized diode laser with the zeeman shift in an atomic vapor. *Applied Optics*, 37(15):3295–3298, 1998.

J. Daley, M. Douglas, L. Hambro, and N. M. Kroll. New theoretical values of the 2^3P fine-structure splittings of helium. *Phys. Rev. Lett.*, 29:12–15, 1972.

W. Demtröder. *Laser Spectroscopy.* Springer, 4th edition, 2008.

G. W. F. Drake. *Can. J. Phys.*, 80:1195, 2002.

M. C. George, L. D. Lombardi, and E. A. Hessels. Precision microwave measurement of the $2^3P_1 - 2^3P_0$ interval in atomic helium: A determination of the fine-structure constant. *Phys. Rev. Lett.*, 87:173002, 2001.

R. Giannini, E. Breschi, C. Affolderbach, G. Bison, G. Mileti, H. P. Herzig, and A. Weis. Sub-doppler diode laser frequency stabilization with the DAVLL scheme on the D_1 line of a ^{87}Rb vapor-cell. *14th International School on Quantum Electronics: Laser Physics and Applications*, 6604:1–5, 2007.

G. Giusfredi, P. Cancio Pastor, P. De Natale, D. Mazzotti, C. de Mauro, L. Fallani, G. Hagel, V. Krachmalnicoff, and M. Inguscio. Present status of the fine-structure frequencies of the 2^3P helium level. *Canadian Journal of Physics*, 83(4):301–310, 2005.

D. Hanneke, S. Fogwell, and G. Gabrielse. New measurement of the electron magnetic moment and the fine structure constant. *Phys. Rev. Lett.*, 100:120801, 2008.

K. Pachucki and J. Sapirstein. *Journal of Physics B: Atomic, Molecular and Optical Physics*, 36:803, 2003.

K. Pachucki and V. A. Yerokhin. *Journal of Physics: Conference Series*, 264: 012007, 2011.

K. Pachucki, V. A. Yerokhin, and P. Cancio Pastor. Quantum electrodynamic calculation of the hyperfine structure of ^{3}He. *Phys. Rev. A*, 85:042517, 2012.

F. M. J. Pichanick, R. D. Swift, C. E. Johnson, and V. W. Hughes. Experiments on the 2^3P state of helium. I. A measurement of the $2^3P_1 - 2^3P_2$ fine structure. *Phys. Rev.*, 169:55–78, 1968.

N. F. Ramsey. A new molecular beam resonance method. *Phys. Rev.*, 76:996–996, 1949.

W. Rooijakkers, W. Hogervorst, and W. Vassen. An intense collimated beam of metastable helium atoms by two-dimensional laser cooling. *Optics Communications*, 123(1–3):321–330, 1996.

M. Smiciklas and D. Shiner. Determination of the fine structure constant using helium fine structure. *Phys. Rev. Lett.*, 105:123001, 2010.

C. H. Storry and E. A. Hessels. Precision microwave measurement of the $2^3P_1 - 2^3P_0$ interval in atomic helium. *Phys. Rev. A*, 58:R8–R11, 1998.

C. H. Storry, M. C. George, and E. A. Hessels. Precision microwave measurement of the $2^3P_1 - 2^3P_2$ interval in atomic helium. *Phys. Rev. Lett.*, 84:3274–3277, 2000.

F. Träger. *Springer Handbook of Lasers and Optics.* Springer, 2007.

J. R. Woodworth and H. W. Moos. Experimental determination of the single-photon transition rate between the 2^3S_1 and 1^1S_0 states of He I. *Phys. Rev. A*, 12:2455–2463, 1975.

T. Zelevinsky, D. Farkas, and G. Gabrielse. Precision measurement of the three 2^3P_J helium fine structure intervals. *Phys. Rev. Lett.*, 95:203001, 2005.